Aerosol radiative effects and feedbacks on boundary layer meteorology and $PM_{2.5}$ chemical components during winter haze events over the Beijing-Tianjin-Hebei region

Jiawei Li[1], Zhiwei Han[*1,2], Yunfei Wu[1], Zhe Xiong[1], Xiangao Xia[3], Jie Li[1,2], Lin Liang[1,2], Renjian Zhang[1]

[1] Key Laboratory of Regional Climate-Environment for Temperate East Asia, Institute of Atmospheric Physics, Chinese Academy of Sciences, Beijing 100029, China
[2] University of Chinese Academy of Sciences, Beijing 100049, China
[3] Key Laboratory of Middle Atmosphere and Global Environment Observation, Institute of Atmospheric Physics, Chinese Academy of Sciences,
Beijing100029, China
Correspondence to: Zhiwei Han (hzw@mail.iap.ac.cn)

Abstract

An online-coupled regional chemistry/aerosol-climate model (RIEMS-Chem) was developed and utilized to investigate the mechanisms of haze formation and evolution and aerosol radiative feedback during winter haze episodes in February-March 2014 over the Beijing-Tianjin-Hebei (BTH) region in China. Model comparison against a variety of observations demonstrated a good ability of RIEMS-Chem in reproducing meteorological variables, PBL heights, $PM_{2.5}$ and its chemical components, as well as aerosol optical properties. The model performances were remarkably improved for both meteorology and chemistry by taking aerosol radiative feedback into account. The domain average aerosol radiative effects (AREs) were estimated to be -57 W m^{-2} at the surface, 25 W m^{-2} in the atmosphere and -32 W m^{-2} at the top of atmosphere (TOA), respectively, during a severe haze episode (20–26 February), with the maximum hourly surface ARE reaching -384 W m^{-2} in southern Hebei province. The average feedback-induced changes in 2-m air temperature (T2), 10-m wind speed (WS10), 2-m relative humidity (RH2) and planetary boundary layer (PBL) height over the BTH region during the haze episode were -1.8 °C, -0.5 m s^{-1}, 10.0% and -184 m, respectively. The BTH average

changes in $PM_{2.5}$ concentration due to the feedback were estimated to be 20.0 μg m^{-3} (29%) and 45.1 μg m^{-3} (39%) for the entire period and the severe haze episode, respectively, which demonstrated a significant impact of aerosol radiative feedback on haze formation. The relative changes in secondary aerosols were larger than those in primary aerosols due to enhanced chemical reactions by aerosol feedback. The feedback-induced absolute change in $PM_{2.5}$ concentrations was largest in haze persistence stage, followed by those in growth stage and dissipating stage. Process analyses on haze events in Beijing revealed that local emission, chemical reaction and regional transport mainly contributed to haze formation in the growth stage, whereas vertical processes (diffusion, advection and dry deposition) were major processes for $PM_{2.5}$ removals. Chemical processes and local emissions dominated the increase in $PM_{2.5}$ concentrations during the severe haze episode, whereas horizontal advection contributed to the $PM_{2.5}$ increase with a similar magnitude to local emissions and chemical processes during a moderate haze episode on 1–4 March. The contributions from physical and chemical processes to the feedback-induced changes in $PM_{2.5}$ and its major components were explored and quantified through process analyses. For the severe haze episode, the increase in the change rate of $PM_{2.5}$ (9.5 μg m^{-3} h^{-1}) induced by the feedback in the growth stage was attributed to the larger contribution from chemical processes (7.3 μg m^{-3} h^{-1}) than that from physical processes (2.2 μg m^{-3} h^{-1}), whereas, during the moderate haze episode, the increase in the $PM_{2.5}$ change rate (2.4 μg m^{-3} h^{-1}) in the growth stage was contributed more significantly by physical processes (1.4 μg m^{-3} h^{-1}) than by chemical processes (1.0 μg m^{-3} h^{-1}). In general, the aerosol-radiation feedback increased the accumulation rate of aerosols in the growth stage through weakening vertical diffusion, promoting chemical reactions, and/or enhancing horizontal advection. It enhanced the removal rate through increasing vertical diffusion and vertical advection in the dissipation stage, and had little effect on the change rate of $PM_{2.5}$ in the persistence stage.

1 Introduction

Aerosols affect radiation transfer by scattering or absorbing solar and infrared radiation, by acting as cloud condensation nuclei (CCN) to modify cloud properties, and by heating the

atmosphere to alter cloud formation, termed as the aerosol direct radiative effect, indirect effect, and semi-direct effect (Twomey, 1974; Albrecht, 1989; Ramanathan et al., 2001), respectively. In addition, there exists a set of interactions between chemistry, radiation and meteorology (Dawson et al., 2007; Zhang, 2008; Isaksen et al., 2009; Baklanov et al., 2014; Cai et al., 2017), which is highly complex and nonlinear and is currently one of the least understood mechanisms in atmospheric science community. The above interactions are traditionally not included or simplified in meteorological or chemical models, but have now been considered and treated with different degrees of complexity in a few online coupled models along with the advances in our knowledge and computer power, and the coupling of meteorology and chemistry and its feedbacks remains one of the most challenging issues in air quality and climate change (Zhang, 2008; Baklanov et al., 2014).

Rapid and continuous growth of economy and energy consumption in the past decades has greatly elevated aerosol levels in China (Chan and Yao, 2008; Zhang et al., 2012; Li et al., 2017a), resulting in serious air pollution problem and potentially significant influence on radiation and climate at multi-scales. Although emission control strategies have been gradually implemented in recent years, haze events still often occur in east China, especially in the BTH region in wintertime due to both higher anthropogenic emissions and poorer meteorological conditions. The haze issue has attracted wide attentions from public, government and scientific community in China and a lot of monitoring and modeling studies have been carried out to explore the sources, characteristics, formation and evolution mechanisms of haze events at both urban and regional scales (Chan and Yao, 2008; Zhang et al., 2012; Che et al., 2014; Guo et al., 2014; Huang et al., 2014; Sun et al., 2014; Zheng et al., 2015; Cheng et al., 2016; Ding et al., 2016; Li and Han, 2016a; Cai et al., 2017; Fu and Chen, 2017; Li et al., 2017b; Wang et al., 2017; Huang et al., 2018; Zhang et al., 2018a; Zhong et al., 2018a; Zhong et al., 2018b; An et al., 2019; Li et al., 2019a), through which our understanding on haze issue has been promoted. However, there is still a large gap in our knowledge about haze formation mechanism, in particular the role of aerosol-radiation-meteorology feedback in haze formation and evolution (Fu and Chen, 2017; Zhong et al., 2018a; An et al., 2019).

The aerosol radiative feedbacks on air quality and meteorology have ever been studied in American and Europe with regional online coupled meteorology-chemistry models, such as

WRF-Chem (Zhang et al., 2010; Forkel et al., 2012), which demonstrates an important role of the feedback in both air quality and meteorology. Carslaw et al. (2010) also pointed out the complexity and significance of natural aerosol interactions and feedbacks within the Earth system.

In east Asia, Han et al. (2013) revealed a significant feedback of mineral dust on dust deflation and transport, atmospheric dynamics, cloud and precipitation in spring and an improvement of model prediction for PM (particulate matter) concentration and surface meteorology by the inclusion of the feedback effect into an online coupled chemistry-aerosol-climate model. In recent years, given the increasing concerns on severe PM pollution during haze days, some modeling studies have been conducted to investigate the effect of aerosol radiative feedback on meteorology and near surface $PM_{2.5}$ concentration, with focus on winter haze events in north China (Wang et al., 2014a; Wang et al., 2014b; Zhang et al., 2015; Gao et al., 2015; Gao et al., 2016; Qiu et al., 2017; Zhao et al., 2017; Zhang et al., 2018b; Chen et al., 2019; Wu et al., 2019). Most of the model results exhibited a positive feedback which tended to increase $PM_{2.5}$ level, but the magnitude of such feedback differs largely, with the mean fractional change in $PM_{2.5}$ concentration varying from just a few percentage (Kajino et al., 2017; Wu et al., 2019) to around 30% (Wang et al., 2014a). Some studies even show a negative feedback on $PM_{2.5}$ in Beijing (Zhang et al., 2015; Gao et al., 2016). Recently, Gao et al. (2020) reported that the aerosol–radiation feedback-induced daytime changes in $PM_{2.5}$ concentrations were less than 6% during haze days in the BTH region in January 2010 from six applications of different online coupled meteorology-chemistry models under the international framework of the MICS-Asia (Model Inter Comparison Study for Asia) Phase III. There existed some differences in the above modeling studies in terms of study period and haze level, although they were all for winter haze events in the BTH region. Zhong et al. (2018a) reported that over 70% of $PM_{2.5}$ increase during cumulative explosive stage of haze event in Beijing in winter can be attributed to the feedback effect based on integrated analysis of observations. The above studies highlight the importance and large uncertainties in the aerosol radiative feedback, which require further model development and investigation.

The diversity in the feedback effect among models could be associated with the differences in the predictions of aerosol chemical components and aerosol optical properties, the

assumption of mixing state and hygroscopic growth scheme, as well as meteorological fields, all of which determine the direction and magnitude of the feedback effect. Majority of previous model studies underpredicted PM concentrations in the north China Plain, especially for aerosol components, such as sulfate, nitrate and SOA concentrations, mainly due to incomplete understanding and unrealistic treatment of secondary aerosol formation through multi-phase chemical processes. Gao et al., (2018) reported that most of the participating models (including WRF-Chem) in the MICS-Asia (Model Inter Comparison Study for Asia) project underpredicted inorganic and organic aerosol concentrations by up to a factor of three. Besides aerosol mass concentration, the unrealistic representation of aerosol properties, such as composition, size distribution, mixing state, hygroscopic growth would also lead to model biases in aerosol optical properties and direct radiative effects. The low biases in the predicted aerosol compositions may lead to underpredictions of aerosol optical depth (AOD) and consequently of aerosol radiative effects and feedback. Che et al. (2014) reported a reduction of solar radiation by aerosols exceeding 200 W m^{-2} during a severe haze event in the north China Plain, much stronger than the estimations from models (around -100 W m^{-2}). Therefore, a realistic treatment and an accurate representation of aerosol processes and properties are crucial to the estimation of aerosol radiative effects and feedback.

It has been well recognized that high aerosol loadings can apparently reduce incoming solar radiation at the surface, leading to surface cooling and inversion associated with reduced wind speed and vertical diffusivity, and consequently increase in surface aerosol concentrations. However, while we have gained considerable knowledge on the overall feedback effect of aerosols, the detailed processes involved in the feedback mechanism are still poorly understood and barely quantified, for example, how does the aerosol radiative effect modify meteorological variables? how do the radiative and meteorological changes affect physical and chemical processes and in turn affect the magnitude and distribution of aerosol components? how to quantify the relative contributions from various physical and chemical processes to the feedback effect?

In this study, an online coupled regional climate-chemistry-aerosol model (RIEMS-Chem) was developed and applied to explore the formation and evolution of haze events during February-March 2014, in which a week-long haze episode with the daily maximum $PM_{2.5}$

concentration up to 400 μg m^{-3} (hourly mean up to 483 μg m^{-3}) was observed. A wide variety of field measurements of aerosol chemical components, optical properties, as well as meteorological variables were conducted and applied to develop, constrain and validate the model. The mechanisms of haze formation and evolution, aerosol radiative effects and feedback on meteorology and chemistry were investigated and assessed. The overall aerosol feedback on $PM_{2.5}$ and its aerosol compositions and the individual contributions to the feedback from physical and chemical processes (advection, diffusion, deposition, chemistry, etc.) during haze events were interpreted and quantified by a process analysis approach incorporated in the model. The results from this study are expected to provide new insights into the mechanism of aerosol-radiation-meteorology feedback, which is currently the source of one of the largest uncertainties in haze formation and evolution.

2 Model and Data

2.1 Model description

An online-coupled regional atmospheric chemistry/aerosol-climate model RIEMS-Chem was used in this study, which was developed based on the Regional Integrated Environmental Model System (RIEMS) (Fu et al., 2005; Wang et al., 2015). A series of modules and parameterizations were adopted to represent major physical processes, including a modified Biosphere-Atmosphere Transfer Scheme (BATS; Dickinson et al., 1993) to simulate land surface process, the Medium-Range Forecasts scheme (MRF) to represent the planetary boundary layer process (Hong and Pan, 1996), the cumulus convective parameterization scheme from Grell (1993), and a modified radiation package of the NCAR Community Climate Model, version CCM3 (Kiehl et al., 1996) to represent radiation transfer process including aerosol effect. RIEMS had been applied to investigate East Asian monsoon climate and the interactions among physical, biological and chemical processes (Xiong et al., 2009; Zhao, 2013; Wang et al., 2015). RIEMS had participated in the Regional Climate Model Intercomparison Project (RMIP) for Asia and it was one of the best models in predicting air temperature and precipitation over east Asia (Fu et al., 2005).

The online-coupled model RIEMS-Chem has been developed in recent years by

incorporating major atmospheric chemistry/aerosol processes into the host model. Transport of pollutants are driven by meteorological fields from RIEMS and changes of pollutants exert feedbacks on the existing dynamic and physical modules (Han, 2010; Han et al., 2012). Major atmospheric processes including emission, advection, diffusion, multi-phase chemistry, dry deposition and wet scavenging of pollutants are considered. The advection and diffusion for pollutants are treated with the same scheme for substances (such as moisture). Gas phase chemistry is represented by an updated Carbon-bond mechanism (CB-IV; Gery et al., 1989). The aerosol effect on photolysis rate is considered by using the Tropospheric Ultraviolet-Visible (TUV) radiation model (Lee-Taylor and Madronich, 2007). Thermodynamic processes are calculated by the ISORROPIA II model (Fountoukis and Nenes, 2007). Dry deposition velocity of aerosol is calculated by a size-dependent scheme which is expressed as the inverse of the sum of resistance plus a gravitational settling term, while below-cloud wet scavenging of aerosol is parameterized as a function of precipitation rate and collision efficiency of particle by hydrometeor (Han et al., 2004). Heterogeneous reactions between gases and mineral dust and sea salt aerosols have also been incorporated into RIEMS-Chem (Li and Han, 2010; Li et al., 2018a). SOA formation is parameterized by a two-product model (Odum et al., 1997).

Current atmospheric chemistry models generally tend to underpredict sulfate concentrations, especially in source regions during wintertime, such as north China, which could be due to uncertainties in the treatment of chemical formation mechanism. Recent model studies suggested that heterogeneous reactions could be an important pathway in sulfate formation during winter haze episodes in north China (Li et al., 2017c; Li et al., 2018b). Therefore, heterogeneous reactions concerning the conversion of SO_2 to sulfate on pre-existed hydrated aerosols were incorporated in RIEMS-Chem. The method of Li et al. (2018b) was adopted, in which the uptake coefficient (γ_{so2}) was a stepwise function determined by the aerosol liquid water content (ALWC) which was predicted by the ISORROPIA II model. Accordingly, the upper bound of ALWC was set to 300 μg m^{-3} ($\gamma_{so2}=1\times10^{-4}$) while the lower bound was 30 μg m^{-3} ($\gamma_{so2}=1\times10^{-6}$). γ_{so2} was linearly interpolated between the upper and lower bounds in terms of ALWC.

RIEMS-Chem treats 9 aerosol types including sulfate, nitrate, ammonium, black carbon (BC), primary organic aerosol (POA), secondary organic aerosol (SOA), anthropogenic

primary PMs ($PM_{2.5}$ and PM_{10}), dust and sea salt. The size distribution of the different types of aerosols is previously prescribed based on the OPAC database (Optical Properties of Aerosols and Clouds) (Hess et al., 1998). In this study, measurements in Beijing are used to represent aerosol size distribution more realistically and to constrain the model. During the study period, a scanning mobility particle sizer (SMPS; TSI, Inc., Shoreview, MN, USA) was used to measure aerosol size distribution (Ma et al., 2017) and the geometric mean radius of inorganic, black carbon and organic carbon aerosols were estimated to be 0.1 μm, 0.05 μm and 0.1 μm, with standard deviations of 1.65, 1.6, 1.65, respectively. The above aerosol size information was incorporated into RIEMS-Chem. The deflation of mineral dust is represented by the scheme of Han et al. (2004) with 5 size bins (0.1–1.0, 1.0–2.0, 2.0–4.0, 4.0–8.0, 8.0–20.0 μm). Primary PMs from anthropogenic are also assigned to the 5 size bins.

Recent observational analyses of aerosol mixing state in Beijing (Ma et al., 2012; Wu et al., 2016) indicated that more than 80% aerosols were internally mixed with BC during haze days, whereas about 70% of aerosols were externally mixed with BC in clean days, so an internal mixing assumption was adopted for model simulation because this study focuses on haze events. Recent measurements also exhibited that the geometric mean radius of dry aerosol internal mixture during haze evolution from light-moderate to severe pollution stages just increased slightly from 0.10 μm to 0.12 μm (Ma et al., 2017), so an average of 0.11 μm is chosen for the geometric mean radius of internal mixture, with standard deviation of 1.65.

Aerosol optical parameters including extinction coefficient, single scattering albedo and asymmetry factor were calculated by a Mie-theory based method developed by Ghan and Zaveri (2007). In this method, the optical properties of different types of aerosols are pre-calculated by Mie theory and fitted by Chebyshev polynomials, which are functions of aerosol geometric mean diameter and refractive index:

$$Q = \exp\left[\sum_{k=1}^{10} A_k T_k(x)\right], \quad (1)$$

$$x = \frac{2\log(D_p) - \log(D_{\min}) - \log(D_{\max})}{\log(D_{\max}) - \log(D_{\min})}, \quad (2)$$

where Q represents the aerosol optical properties (such as scattering efficiency). $T_k(x)$ are the Chebyshev polynomial of order k, which is related to particle size, A_k are the Chebyshev

coefficients which is related to refractive index, D_p is the geometric mean diameter, D_{min} and D_{max} are the minimum and maximum D_p for obtaining the Chebyshev polynomials, with values of 0.001 μm and 10 μm, respectively. It has been proved that 40 groups of D_p in the range from D_{min} and D_{max} are sufficient to control errors below 10% compared with classical Mie code calculation.

The effect of water uptake is treated by the κ-Köhler parameterization (Petters and Kreidenweis, 2007), which calculates aerosol wet diameter due to hygroscopic growth under different relative humidity. The bulk κ for internal mixture of aerosols is derived by the volume-weighted average of κ of each aerosol component, while the κ values for inorganic aerosols, BC, POA, SOA, dust and sea salt were set to 0.65, 0, 0.1, 0.2, 0.01 and 0.98, respectively, according to previous observational and modeling studies (Riemer et al., 2010; Liu et al., 2010a; Westervelt et al., 2012):

$$\kappa = \sum_j \frac{V_j}{V_a} \kappa_j , \quad (3)$$

where V_a is the total volume of dry aerosols, V_j is the volume of each aerosol component j.

The refractive index of internally mixed aerosols is calculated using the Maxwell-Garnett mixing rule:

$$R_w^2 = R_s^2 \left[\frac{R_i^2 + 2R_s^2 + 2 f_i (R_i^2 - R_s^2)}{R_i^2 + 2R_s^2 - f_i (R_i^2 - R_s^2)} \right], \quad (4)$$

$$f_i = \frac{V_i}{V}, \quad (5)$$

where R_w is the refractive index of the internal mixture, R_i and R_s are the refractive index of insoluble components (BC and POA) and soluble components (inorganic aerosols, SOA and water), respectively. V_i represents the volume of insoluble components, V represents the total volume of wetted aerosols.

After obtaining the wet diameter (D_p) and refractive index of the internally mixed aerosols (R_w), the aerosol optical properties (Q) can be derived from formula (1) with the Chebyshev fitting coefficients table. Then, aerosol optical parameters, such as extinction coefficient can be obtained through multiplying Q by aerosol mass concentration from chemical module. The advantage of this optical module is the computational speed is much faster than that from the

traditional Mie calculation, with a similar level of accuracy. This module has been successfully used in estimations of aerosol optical properties and direct radiative effects over East Asia (Han et al., 2011a; Li and Han, 2016b; Li et al., 2019b).

An empirical method from Hegg (1994) is applied to link cloud droplet number concentration N_c to mass concentration of hydrophilic aerosols (sulfate, nitrate, hydrophilic BC and OC) to represent the first indirect effect, while the parameterization of Beheng (1994) is used to represent the second indirect effect, in which the autoconversion rate converting from cloud water to rain water depends on N_c and cloud liquid water content W_L. The cloud effective radius r_e is calculated based on N_c, W_L and the cube of the ratio of the mean volume radius and the effective radius of the cloud-droplet spectrum following Martin et al. (1994). The effect of aerosols on ice nuclei and convective cloud is not treated yet in this model because of the complexity and limitation in knowledge.

The aerosol optical parameters and N_c due to aerosol activation calculated above are transferred into radiation module to account for the perturbation of radiation and atmospheric heating rate due to aerosol direct and indirect effects. The subsequently called land surface module and boundary layer module calculate the changes in land-air fluxes of heat and moisture, turbulent diffusion coefficients and meteorological variables in the boundary layer in response to the radiation change, and then air temperature tendency is calculated in terms of the altered atmospheric heating rate and radiation, which further leads to changes in meteorological variables, and in turn affect physical and chemical processes and concentrations of aerosols and their precursors represented in the chemical module. All the physical modules are called every 2.5 minutes and the transfer of variables between chemical module and radiation/meteorological modules is made every 30 minutes.

RIEMS-Chem has been successfully applied in previous modeling studies of anthropogenic aerosols, mineral dust and marine aerosols regarding spatial-temporal distributions, physical and chemical evolutions, radiative and climatic effects over east Asia (Han et al., 2011b; 2012; 2013; 2019; Li et al., 2014; Li and Han, 2016b; 2016c; Li et al., 2019b). RIEMS-Chem has been participating in the international model comparison project Model Inter Comparison Study for Asia phase III (MICS-Asia III) and shows a good ability in predicting $PM_{2.5}$ concentration and AOD over East Asia (Gao et al., 2018).

294

295 2.2 Process analysis

296 In RIEMS-Chem, a time-splitting scheme based on continuity equation is applied to predict
297 species concentrations; therefore, the species concentrations are the net results of successive
298 changes in emissions, dynamic transport, physical and chemical processes and the changes in
299 species concentration by each process can be recorded, allowing the quantification of
300 individual contribution of each process to species variation. In this study, a process analysis
301 (PA) scheme, which calculates the Integrated Process Rates (IPR) at each time step and each
302 grid, was embedded in RIEMS-Chem to identify the contributions of physical and chemical
303 processes to aerosol evolution. At each time step, the IPR for a certain process was calculated
304 by subtracting the species concentrations at the beginning of this process from the ones after
305 the process. The IPR method has ever been applied to study the formation and fate of particulate
306 and gaseous pollutants in North America and China (e.g. Yu et al., 2008; Zhang et al., 2009;
307 Liu et al., 2010b). The processes involved in aerosol evolution include emissions of primary
308 species, advections (horizontal and vertical), diffusions (horizontal and vertical), dry deposition,
309 chemical processes (gas-phase chemistry, aqueous chemistry, thermodynamic equilibrium and
310 heterogeneous reactions), cloud processes and wet deposition. Here cloud process represents
311 the effects of cloud attenuation of photolysis rate, aqueous-phase chemistry and in-cloud
312 mixing. In this study, PA is applied not only to quantify the contributions of individual physical
313 and chemical processes to haze evolution, but also to help interpret the processes involved in
314 aerosol radiative feedback. In addition, different from the previous PA application, chemical
315 processes are further classified into gas phase, thermodynamic and heterogeneous reactions to
316 provide more details on chemical pathways of secondary aerosol formation. The mass balance
317 of IPR has been examined, assuring that the change in species concentration during one time
318 step is equal to the sum of IPRs by each of the processes.

319

320 2.3 Emission inventories

321 Monthly mean anthropogenic emissions of sulfur dioxide (SO_2), nitrogen (NO_x), ammonia
322 (NH_3), non-methane volatile organic compounds (NMVOC), carbon monoxide (CO), black
323 carbon (BC), primary organic carbon (POA), other anthropogenic primary $PM_{2.5}$ and primary

PM_{10} in China for the year 2014 were obtained from the MEIC inventory (Multi-resolution Emission Inventory for China) which was developed by Tsinghua University (http://meicmodel.org). Anthropogenic emissions outside China were taken from the MIX inventory which was developed to support the Model Inter-Comparison Study for Asia phase III (MICS-Asia III) and the Hemispheric Transport of Air Pollution (HTAP) projects (Li et al., 2017a). Both inventories of MEIC and MIX have the horizontal resolution of 0.25 degree. Biomass burning emissions of aerosols and gas precursors for the year 2014 with a horizontal resolution of 0.25 degree were derived from the fourth version of the Global Fire Emissions Database (GFED4) (Giglio et al., 2013). Monthly mean biogenic emissions of isoprene and monoterpene were derived from Global Emissions Inventory Activity (GEIA, http://www.geiacenter.org/). The above emission data were bilinearly interpolated to the lambert projection of RIEMS-Chem.

2.4 Model configuration and numerical experiments

RIEMS-Chem was configured on a lambert conformal projection with horizontal resolution of 60 km, covering most areas of China, the Korean Peninsula, Japan and part of the Indo-China Peninsula (Figure 1). 16 vertical layers distributed vertically and unevenly in the terrain-following sigma coordinate, with the lowest 8 layers within the boundary layer. This study focused on the Beijing-Tianjin-Hebei (BTH) region with more attentions to the Beijing metropolitan. The study period was from 10 February to 12 March, 2014, encountering several haze episodes. The first 7 days were taken as model spin-up and the results from 17 February to 12 March were used for analysis.

Initial and boundary conditions for meteorological variables were provided by the final reanalysis data (FNL) with 1°×1° resolution and 6-hourly interval from the National Centers for Environmental Prediction (NOAA/NCEP, 2000). Lateral boundary conditions of chemical species at 6-hourly interval were derived from the simulations of the global chemical model MOZART-4 (Model for Ozone and Related chemical Tracers, version 4; Emmons et al., 2010).

To investigate the aerosol radiative effects and its potential feedback on solar radiation, meteorological variables, planetary boundary layer (PBL) and aerosol concentrations in the study domain, two simulations were designed. The FULL simulation (with aerosols)

considered all aerosol direct and indirect effects and feedbacks, and the NoAFB simulation shuts off aerosol direct radiative effects and removes anthropogenic aerosols in aerosol indirect effects. In both simulations, the driving meteorological data, emissions and model settings were exactly the same.

2.5 Observational data

Several observational datasets for meteorological variables, aerosol concentrations and aerosol optical parameters were obtained and used for model comparison and analysis.

In-situ 3-hourly observations of temperature at 2 meter (T2), wind speed at 10 meter (WS10) and relative humidity at 2 meter (RH2) from three meteorological monitoring sites around Beijing (Figure 1) were collected from the China Meteorological Data Service Center (CMDS) (http://data.cma.cn/).

To evaluate the model ability in reproducing evolution of planetary boundary layer (PBL), high-frequency sounding data measured around 14:00 LST at the Xianghe station (39°45′N, 116°58′E; approximately 63 km southeast of Beijing downtown) were collected, from which the PBL height can be determined based on the vertical gradients of virtual potential temperature and water mixing ratio according to the method from Heo et al. (2003). This sounding dataset provided a good indicator of mixing layer height because the sounding was launched at 14:00 LST and lasts for about one hour. The meteorological sounding was launched in Xianghe once a week (every Tuesday) and totally four soundings were available during the study period (18 and 25 February, 4 and 11 March). Fortunately, the four soundings encountered one severe haze episode, one moderate haze episode, and two clean days, providing robust evidences on day-to-day variation of mixing layer height under various atmospheric conditions. Hourly downward shortwave radiation flux (SWDOWN) at the surface was measured simultaneously at the Xianghe station by a pyranometer with sun shield and was used in this study.

The measurements of mass concentrations of $PM_{2.5}$ and its components and aerosol optical parameters were carried out at the tower division of the Institute of Atmospheric Physics (IAP), Chinese Academy of Sciences (CAS) in Beijing (39°58′N, 116°22′E) from 17 February to 12 March, 2014. Real-time hourly $PM_{2.5}$ mass concentrations were online measured by a hybrid

beta attenuation particulate monitor (Model 5030 SHARP, Thermo Scientific, USA). $PM_{2.5}$ samples were collected in parallel by an R&P Partisol®Model 2025 dichotomous sequential PM air sampler (Thermo, USA) and a MiniVol TAS PM sampler (Airmetrics, USA) between 24 February and 12 March, 2014. Samples were collected twice per day with one during the daytime (from 7:00 to 19:00 LST) and the other at night (from 19:00 to 7:00 of the next day). Totally 33 half-day samples were collected. Aerosol chemical compositions including sulfate (SO_4^{2-}), nitrate (NO_3^-), ammonium (NH_4^+), BC and OC were analyzed by ion chromatography (Dionex ICS-90 for cations and ICS-1500 for anions) and a DRI-2100A carbonaceous aerosol analyzer. Real-time hourly aerosol extinction coefficient and aerosol absorption coefficient at dry condition (RH=10%) were synchronously measured by a nephelometer (Aurora3000) and an aethalometer (AE-31), respectively. Detailed information about this experiment including the sampling site, instruments, measurement procedures and sample analysis were well documented in Ma et al. (2017). The mass concentration of SOC was estimated using a revised EC tracer method (Zhao et al., 2013).

Measurements of AOD at the 4 sites (Nanjiao, Tianjin, Gucheng and Shangdianzi) in the BTH region were obtained from the China Aerosol Remote Sensing Network (CARSNET) (Che et al., 2014). Nanjiao is an urban site located in southern Beijing. Tianjin site is located in the center of Tianjin city, about 120 km to the southeast of Beijing. Gucheng, a suburban site in Hebei province, is about 130 km to the southwest of Beijing downtown. Shangdianzi is located 150 km to the northeast of Beijing, which is a background station since it is far away from anthropogenic sources. Daily mean AOD was derived by temporally averaging the raw data measured by sunphotometer during daytime. To compare with the model output, AOD at 550 nm was used.

3 Model validations

3.1 Meteorological variables

Wind speed, temperature and relative humidity are key meteorological factors affecting physical and chemical processes of atmospheric pollutants. The statistics for comparison between in-situ observation and the FULL simulation for WS10, T2 and RH2 are presented in

Table 1. At the 3 sites (Beijing, Tianjin and Tanggu), the model performances were reasonably good, although wind speeds were somewhat overpredicted. The overall correlation coefficient (R) and normalized mean bias (NMB) at the 3 sites were 0.83 and -2% for T2, 0.61 and -1% for RH2 and 0.47 and 31% for WS10. In all, RIEMS-Chem was able to reasonably reproduce the meteorological variables during the study period. The statistics for NoAFB simulation are also list in Table 1. It is noteworthy that the statistics for the FULL simulation are overall better than those for NoAFB simulation, such as the warm bias in the simulated air temperature and positive bias in wind speed are apparently reduced. This demonstrates the inclusion of aerosol radiative effects does improve meteorological prediction in this study.

The observed hourly SWDOWN in Xianghe was compared with model simulation (Figure 2a). In general, the FULL case well reproduced SWDOWN in clean days and light-moderate polluted days, but tended to underpredict observations in heavy haze days, such as the period from 20 to 26 February. Underpredictions of cloud amount and PM concentrations could be reasons for the low bias. For the entire study period, the observed and simulated (FULL) mean SWDOWN were 136.0 W m^{-2} and 188.4 W m^{-2}, respectively, with R of 0.91 (Figure 2a). If only days with low cloud covers were considered, the SWDOWNs were 183.3 W m^{-2} and 213.7 W m^{-2} from observation and the FULL case, respectively, with the NMB of 16%. In contrast, the NoAFB case failed to capture the decreasing tendency of SWDOWN during haze days, resulting in a larger bias (NMB of 72%) than the FULL case.

To examine the model performance for meteorology in the vertical direction, we collected meteorological sounding data at Beijing observatory from the website of University of Wyoming (http://weather.uwyo.edu/upperair/sounding.html). Figure S1 and S2 present the average observed and simulated vertical profiles of air temperature, wind speed and relative humidity at 08:00 LST and 20:00 LST during the two haze episodes of 20-26 February and 1-4 March 2014 and the corresponding comparison statistics for these variables in the troposphere and at altitudes below 3 km are listed in Tables S1 and S2. In general, the model is able to generally capture the major features of vertical distribution of key meteorological variables, although the model tends to predict higher relative humidity in the middle-upper troposphere. Such overpredictions are also found for the same region in previous studies, such as WRF-Chem simulation (Gao et al., 2016). The statistics indicate that the model simulated vertical

distribution of meteorological variables are within an acceptable accuracy range of current meteorological model predictions.

3.2 Planetary boundary layer (PBL) height

Figure 2b shows the simulated PBL heights at 14:00 LST from the FULL case and NoAFB case during the study period and the observed PBL heights at 14:00 LST determined from air soundings on 18 February (clean), 25 February (severe haze), 4 March (clean) and 11 March (haze), 2014, respectively. There was large variation in PBL height in the afternoon, with higher PBL height in clean days and lower one in haze days, inversely related to the $PM_{2.5}$ level. The FULL case well reproduced the very low PBL height during the most severe haze episode on 25 February, with the observed and simulated PBL heights to be 569 m and 587 m, respectively. In clean days, the much higher mixing layer was also well captured, such as, on 4 March, the observed and simulated PBL heights were 2305 m and 2535 m, respectively. It is noteworthy that the simulated PBL heights in the NoAFB case were consistently higher than those in the FULL case, and the PBL height simulation from the FULL case (considering aerosol radiative effects) was apparently in a better agreement with observation than that from the NoAFB case, except for that on 18 February.

3.3 Mass concentrations of $PM_{2.5}$ and aerosol components

Figure 2c shows the hourly $PM_{2.5}$ mass concentrations observed at the IAP site and those from the FULL simulation and NoAFB simulation. The study period was characterized by three haze episodes, which was the episode 1 on 20–26 February, the episode 2 from 1 to 4 March, and the episode 3 from 8 to 11 March. The first episode experienced the most severe pollution with the maximum hourly $PM_{2.5}$ concentration exceeding 480 μg m^{-3} on 25 February. The second and third ones were moderately polluted in terms of magnitude and lasting time. In general, the model reproduced the hourly variation of $PM_{2.5}$ concentrations reasonably well in the FULL case, although the peaks were somewhat underpredicted in some days, which could be partly due to the overprediction of wind speed (Table 1) and potential uncertainties in emission inventories. The low bias in $PM_{2.5}$ concentrations could also contribute to the overprediction of SWDOWN during the first haze episode (20-26 February) discussed in

section 3.1. The average $PM_{2.5}$ concentrations during the study period were 142.0 μg m^{-3} and 131.4 μg m^{-3} from observation and the FULL simulation, respectively, with R of 0.8 and NMB of -7% (Table 2), which demonstrates a good model performance for $PM_{2.5}$ predictions for the winter haze periods. A remarkable feature shown in Figure 2 is the significant negative correlation between $PM_{2.5}$ concentration and PBL height and SWDOWN.

The comparison between the simulated daily mean surface aerosol components (sulfate (SO_4^{2-}), nitrate (NO_3^-), ammonium (NH_4^+), BC and OC) and observations at the IAP site are presented in Figure 3. The daily mean observation in the figure is an average of the half-day samples, while the original half-day samples are used for statistics calculation in Table 2. The model (from the FULL case) generally exhibits a good performance for inorganic aerosol (sulfate, nitrate and ammonium) concentrations in terms of both daily variation and magnitude (Figure 3a - 3c). It is encouraging that the maximum values on 25 February during the first haze episode and the moderate values on 3 March in the second haze episode are well reproduced, although some low biases occurred in the last few days. On average, the model simulations of 20.3 μg m^{-3}, 24.3 μg m^{-3} and 13.9 μg m^{-3} are very close to the observations of 21.0 μg m^{-3}, 26.0 μg m^{-3} and 14.1 μg m^{-3} for sulfate, nitrate and ammonium, respectively, with Rs of 0.92, 0.88 and 0.91 and NMBs of -4%, -6% and -2%, respectively (Table 2). Most of the online coupled models tended to underpredicted sulfate concentration (Gao et al., 2016; Qiu et al., 2017; Gao et al., 2018), which led to an underestimation of aerosol optical depth and radiative effect. The model in this study improves the simulation of inorganic aerosols, mainly through the inclusion of heterogeneous chemical reactions for inorganic aerosols.

The model also reproduced the temporal variation and magnitude of BC (Figure 3d) and OC (Figure 3e) concentrations in Beijing reasonably well. However, the model tended to underpredict the peak OC values on 24–25 February and to overpredict BC concentrations from late February to early March. The low bias in OC simulation during the haze episodes could be attributed to the underprediction of SOC (Figure 3f) due to potentially missing chemical pathways. Uncertainties in the emission inventory could also be a reason. Li et al., (2017a) reported the uncertainties in BC and OC emissions for China could be ±200%, larger than those of emissions for gases (<70%) and primary PMs (~130%). The period mean BC concentrations from observation and simulation were 5.2 μg m^{-3} and 6.7 μg m^{-3}, respectively, with R of 0.92

and NMB of 28% (Table 2). The period mean simulated and observed POC concentrations were 18.4 μg m^{-3} and 15.5 μg m^{-3}, respectively, with R of 0.93, whereas the simulated SOC concentration was 9.9 μg m^{-3}, lower than observation (13.6 μg m^{-3}) by 27%, with a correlation coefficient of 0.56. For OC (sum of POC and SOC), the simulated value (28.3 μg m^{-3}) was very close to the observation (29.1 μg m^{-3}), with R of 0.88 and NMB of -3%, respectively, which indicated a generally good model performance for the total OC concentration.

It is noteworthy that by considering aerosol radiative effects, the model apparently improved simulations for both $PM_{2.5}$ and its chemical compositions, which is illustrated by comparing model results between the FULL and NoAFB cases (Figure 2c, Figure 3 and Table 2). Another important finding is that the duration of haze episode was prolonged by about 2–3 hours by the aerosol radiative feedback compared with that without aerosol feedback (Figure 2c).

To evaluate the overall model performance on $PM_{2.5}$ and its gas precursors in the BTH region, we also collected observations at 80 surface stations in 13 cities of the BTH from the website of CNEMC (China National Environmental Monitoring Center) (http://www.cnemc.cn/) and made a detailed comparison between observations and model simulations for $PM_{2.5}$, O_3, NO_2 and SO_2. The observed and simulated hourly mass concentrations of these species in the typical cities are presented in Figure S3 - S8 and the statistics for each city and for all the cities are presented in Table S3. The overall model ability is generally satisfactory, with Rs of 0.87, 0.81, 0.60 and 0.74, NMBs of -0.4%, -11%, -17% and 0.5% for $PM_{2.5}$, O_3, SO_2 and NO_2, respectively, for all the sites in the BTH region.

3.4 Aerosol optical parameters

Figure 4a and 4b show the measured and simulated hourly aerosol extinction coefficient (EXT) and aerosol absorption coefficient (ABS) at an RH of 10% at the IAP site during the study period. It clearly showed that the model was able to well reproduce the magnitudes and temporal variations of EXT and ABS under dry condition in the FULL case, although the model tended to predict higher ABS in some days possibly due to the overprediction of BC concentration. Single scattering albedo (SSA) which is defined as the ratio of scattering coefficient (EXT minus ABS) to extinction coefficient is also given in Figure 4c. The FULL

case generally simulated high SSA values during haze episodes, such as 0.92 on 20–26 February, 0.85–0.9 from 1 to 4 March and 0.8–0.9 on 8–11 March, suggesting a dominant role of light scattering aerosols in haze days. It is encouraging that the model reproduced SSA during the severe haze episode (on 20–26 February) quite well, with both the simulation and observation being approximately 0.92. However, SSA observation in clean days (such as on 5–7 March) was lower than that in haze days, and the model tended to overpredict SSA in clean days, which could be attributed to uncertainties in measurement. In clean days, both the denominator (EXT) and numerator (EXT minus ABS) were small, a subtle perturbation in EXT and/or ABS can result in a large variation in SSA. A previous observational study in Beijing suggested that SSA observation was more uncertain in clean days than in polluted days because the observed aerosol extinction coefficient was too low in clean days (Jing et al., 2015). On average, the observed EXT, ABS and SSA values were 0.51 km^{-1}, 0.048 km^{-1} and 0.85, respectively, whereas, the corresponding FULL simulations were 0.53 km^{-1}, 0.052 km^{-1} and 0.88, with Rs of 0.8, 0.7 and 0.7 and NMBs of 4%, 10% and 5%, respectively (Table 2). The above comparison demonstrates a good ability of the model in estimating aerosol optical properties during the study period, which could be attributed to both the good performance for aerosol compositions and the realistic representation of aerosol properties (aerosol size distribution, mixing state, hygroscopic growth etc.), which is based on real-time measurements in Beijing.

Besides EXT and ABS measured under dry condition, measurements of AOD at the four CARSNET sites around Beijing (Nanjiao, Tianjin, Gucheng and Shangdianzi) were also used to evaluate the model ability in simulating aerosol optical parameters in real atmosphere (Figure 5). At the Nanjiao site, which is about 50km southeast of Beijing downtown (Figure 5a), AOD measurement was unavailable in most days during the first haze episode (20 to 26 February), with only two data (around 4.8) available on 25 February. The simulated daily AOD from the FULL case varied from 3.1 to 4.0 during 24 - 26 February, somewhat lower than the observation. The model tended to simulate lower AOD during the third haze episode (8 to 11 March), which can be partly attributed to the predicted lower aerosol concentrations. The measured AODs in Gucheng (southwest to Beijing) and Tianjin were similar in terms of variation and magnitude (Figures 5b and 5c), showing high values during pollution periods

with the maximum daily AOD exceeding 4.0 in Gucheng and 3.5 in Tianjin. The FULL case reproduced the AOD variations and magnitudes reasonably well at the two sites although low biases still occurred during 8 to 11 March in Gucheng. For the regional background site Shangdianzi (Figure 5d), the magnitude and variation of AOD were similar to those in Nanjiao, suggesting that the haze episodes were regionally distributed because the temporal variations and magnitudes of AOD were generally consistent at the four sites.

Table 3 summaries the performance statistics for daily mean AOD. In general, the model reproduced the temporal variation and magnitude of AOD around Beijing reasonably well with the overall R of 0.81 (0.67–0.90) and NMB of -8.6% (-15.6%–6.2%). The underestimation is mainly contributed by the low biases during the third haze episode (8 to 11 March) when inorganic aerosol concentrations were underestimated (Figure 3a–3c). In addition, the limitation in AOD samples during the severe haze episode in Nanjiao and Shangdianzi could amplify the negative bias. At the Gucheng and Tianjin sites where more samples were available, the mean measured AODs were 1.7 and 1.4, respectively, agreeing well with the simulated values of 1.5 and 1.3 from the FULL case.

In summary, the above comparisons demonstrate that RIEMS-Chem was capable in reproducing the spatial distribution and temporal variation of meteorological variables (air temperature, wind speed, surface shortwave radiation, PBL height etc.), concentrations of total $PM_{2.5}$ mass and its chemical compositions and aerosol optical properties during the winter haze periods around Beijing. It is also noteworthy that the inclusion of aerosol radiative effects apparently improved the overall model performance for both meteorological variables and aerosol physical and chemical properties, highlighting the necessity to develop online coupled chemistry-meteorology model for both air quality and climate research. The good agreement above increases confidence in the reliability of the following model results on aerosol radiative effects and feedback.

4 Aerosol radiative effects and feedbacks

4.1 Distributions of meteorological variables and near surface $PM_{2.5}$ concentration

The period-mean distributions of near-surface wind speed (WS10), temperature (T2),

relative humidity (RH2), PBL height and $PM_{2.5}$ concentration are shown in Figures 6a to 6e. During the study period, westerly winds dominated the northwestern parts of the BTH region while southeasterly prevailed over the southeastern parts, as a result, the near-surface wind speeds were fairly weak over the convergence zone from southern Hebei province to Beijing (Figure 6c). Such wind pattern indicated that pollutants from southern parts of the domain (such as Shandong and Henan provinces) can be transported northward to Beijing, Tianjin and Hebei, and air pollutants over the weak-wind regions were easily accumulated to high level. Near-surface temperature showed an apparent south-to-north gradient, with surface air temperature in a range of 4 °C to 6 °C over the southern BTH region, -2 °C to 2 °C in the vicinity of Beijing and parts of central Hebei, and lower than -2 °C in northern parts of the domain (Figure 6a). Relative humidity was higher (~65% to 75%) over northern areas and lower (~55% to 65%) over southern areas (Figure 6b). PBL height also exhibited an apparent gradient in spatial distribution (Figure 6d), ranging from 800-1000 m in northern Hebei and Inner Mongolia to about 600-700 m in southern Beijing, Tianjin and southern Hebei. A belt of high $PM_{2.5}$ concentration spread from southwest to northeast (Figure 6e), with the maximum value up to 150 μg m^{-3} in the vicinity of Shijiazhuang and Beijing and Tianjin. The regions with high $PM_{2.5}$ concentrations generally corresponded well to the weak-wind areas shown in Figure 6c.

Averaged over the BTH region and the entire study period, the simulated T2, WS10, RH2, PBL height and $PM_{2.5}$ concentration from the FULL case were 0.61 °C, 1.2 m s^{-1}, 67.0%, 698.4 m and 90.0 μg m^{-3}, respectively. According to the "Technical Regulation on Ambient Air Quality Index" prescribed by Chinese Ministry of Environmental Protection in 2012, a pollution event occurs when 24-hr mean $PM_{2.5}$ concentration ≥ 75 μg m^{-3}. Totally, there were 11 days with domain and daily average $PM_{2.5}$ concentration exceeding 75 μg m^{-3} in the BTH region, with the maximum exceeding 136 μg m^{-3}, indicating the severity of air pollution during the study period.

4.2 Distributions of AOD, SSA and aerosol radiative effects

Figure 6f shows that high AODs mainly distributed from northern Beijing to southwestern Hebei, southern Shanxi and northern Henan provinces, with the maximum up to 1.1. As AOD was determined by vertical profiles of aerosol compositions and RH, the spatial distribution of

AOD was somewhat different from that of $PM_{2.5}$ concentration. During the study period, the regional mean AOD in the BTH region was 0.78 (Table 4), about twice the long-term observed value of about 0.4 in February and March in the same region (Song et al., 2018).

The simulated SSAs were above 0.88 in the BTH region (Figure 6g), with relatively lower values (0.88 - 0.9) in the areas of high $PM_{2.5}$ concentration and higher ones (0.92 - 0.98) in the relatively clean areas. On average, the simulated SSA in the BTH was 0.91 (Table 4), within the range of 0.87 to 0.95 measured in the same region in January 2013 (Che et al., 2014) but slightly lower than the model simulated annual mean of 0.95 over eastern China (Zhuang et al., 2013).

All-sky aerosol radiative effects at the surface (ARE_{surf}), at the top of atmosphere (ARE_{TOA}) and in the atmosphere (ARE_{atm}) under all-sky condition are presented in Figures 6h to 6j. During the study period, aerosols induced a negative ARE both at the surface and TOA and a positive ARE in the atmosphere over the BTH. The distribution of ARE resembles that of AOD, generally showing stronger effects over southwestern Hebei, Shanxi and northern Henan provinces where high AOD occurred. Moderate AREs appeared over Beijing, Tianjin and central Hebei, while relatively weak AREs appeared over the northern domain. The domain average AREs in the BTH region during the period were estimated to be -37 W m^{-2}, 19 W m^{-2} and -18 W m^{-2} at the surface, in the atmosphere and at the TOA, respectively (Table 4). The indirect radiative effect was also estimated to be about -2 W m^2 at the surface and the TOA on average, much smaller than the direct radiative effect; therefore, the total aerosol radiative feedback is predominated by direct radiative effect during the study period.

The domain average all-sky AREs during the first haze episode (20-26 February) were -57 W m^{-2}, 25 W m^{-2} and -32 W m^{-2} at the surface, in the atmosphere and at the TOA, respectively, and the values were further enhanced to -123 W m^{-2}, 53 W m^{-2} and -70 W m^{-2} in terms of daytime mean. The maximum AREs at the surface and at TOA reached -384 W m^{-2} and -231 W m^{-2}, respectively, at 13:00 LST on 23 February in the vicinity of Shijiazhuang.

In Beijing, the estimated mean AREs were -70 W m^{-2}, 32 W m^{-2} and -38 W m^{-2} at the surface, in the atmosphere and at the TOA, respectively, during the first haze episode, whereas the maximum ARE at the surface reached -304 W m^{-2} at 13:00 LST on 22 February, which was associated with the high $PM_{2.5}$ concentration (453 μg m^{-3}) at that time.

Based on in-situ surface measurements, Che et al. (2014) estimated that during haze periods in January 2013, the mean daytime AREs at Nanjiao and Xianghe were approximately -42 W m^{-2} and -50 W m^{-2} at TOA, and -120 W m^{-2} at the surface at both sites. In this study, the daytime AREs averaged over the severe haze period (20–26 February) at TOA were estimated to be -77 W m^{-2} and -74 W m^{-2} at Nanjiao and Xianghe, while the corresponding AREs at the surface were -146 W m^{-2} and -140 W m^{-2}, respectively. Che et al. (2014) also reported the maximum daily mean surface ARE of -220 W m^{-2} at Nanjiao during a severe haze episode in January 2013, in this study, the corresponding ARE was estimated to be approximately -200 W m^{-2} at the same site during the severe haze episode in February 2014. Therefore, the magnitudes of AREs during haze episodes simulated from this study agreed favorably with the above observational based estimations around Beijing, despite the different time period.

4.3 The feedback effects on meteorological variables and aerosols

Figure 7a–7e shows the mean differences in T2, RH2, wind speed, PBL height and near surface $PM_{2.5}$ concentration induced by the radiative feedback due to all aerosols (FULL minus NoAFB) in the domain during the study period.

The aerosol radiative effects led to a reduction in surface shortwave radiation and thus surface air temperature in the entire domain. The magnitude of T2 variation decreased from south to north of the BTH, with -1.6 °C to -2 °C in southern Hebei and -1.2 °C to -1.8 °C in southern Beijing, respectively. Correspondingly, RH2 increased by 10%-16% in the above regions. The changes in wind speed showed a patchy pattern, with decreases by ~0.1 m s^{-1} in southern Hebei, increases by ~0.2 m s^{-1} in central Hebei, and decreases in most parts of Beijing. Wind vector shows an anomalous northerly wind of ~0.5 m s^{-1} in the BTH region. Due to the reduction in surface shortwave radiation, PBL height decreased over the entire region, with the maximums up to 240 m in southern Hebei and northern Tianjin. The changes in PBL height varied from -210 m in southern Beijing to -90m in northern Beijing. $PM_{2.5}$ concentrations were consistently enhanced over the entire region, with the maximum increase up to 33 μg m^{-3} in southern Hebei and portions of Beijing and Tianjin. In most of the BTH region, the percentage increase of $PM_{2.5}$ exceeded 25%, with the maximum increase exceeding 33% in the vicinity of Shijiazhuang. It is of interest that the regions with the maximum increase of $PM_{2.5}$ generally

corresponded to those with the maximum decrease in PBL height. The presence of aerosols reduced solar radiation reaching the ground surface, resulting in decreases in surface air temperature and PBL height and an increase in relative humidity, all of which favored accumulation and formation of aerosols due to weakened vertical mixing and enhanced secondary aerosol formation.

The aerosol feedback during the first haze episode was further explored due to the much higher $PM_{2.5}$ level than the period average. Figure 7f–7j show the mean changes in meteorological variables and $PM_{2.5}$ concentrations during the first haze episode (20-26 February). In general, the changes induced by aerosol feedback were larger during the severe haze episode than those over the entire study period. T2 decreased by 1.8 °C to 2.7 °C along with an increase up to 20% in RH in southern Hebei and southern parts of Beijing and Tianjin. Different from the entire period average, wind speed decreased consistently in the BTH, with a maximum decrease of 1 m s^{-1}. PBL height decreased by ~300 m in southern Hebei, corresponding to the areas with large air temperature decrease. This resulted in a consistent increase in $PM_{2.5}$ concentrations in the study domain, with the maximum increases exceeding 50% around Shijiazhuang and approximately 40% in Beijing and Tianjin, apparently higher than the entire period averages. If for daytime mean, the percentage changes of $PM_{2.5}$ in the above areas increased to 70% and 60%, respectively (figure not shown). It is striking that the simulated maximum increase in hourly $PM_{2.5}$ concentration can be up to 372 μg/m^3 (186%) in the vicinity of Shijiazhuang at about 10:00 LST on 24 February during the first haze episode, which demonstrates the substantial impact of the radiative feedback on $PM_{2.5}$ concentration and haze formation.

It is worthwhile to further explore the effect of aerosol feedback during haze evolution. We divided haze episode into three stages, the growth stage is defined as the time period of $PM_{2.5}$ increase from clean condition to heavy pollution level, the persistence stage means the duration period of haze and the dissipation stage means the period with a sharp decrease in $PM_{2.5}$ concentration usually along with a cold front passage. During the first heavy haze episode (20–26 February) in Beijing, aerosol radiative feedback caused the increases in $PM_{2.5}$ concentration of 55 μg m^{-3}, 84 μg m^{-3} and 40 μg m^{-3}, with the fractional changes of 31%, 41% and 67%, respectively, during the growth, persistence and dissipation stages. The larger

fractional change of $PM_{2.5}$ in the dissipation stage is due to the relatively large feedback-induced increase and the lowest $PM_{2.5}$ concentration in the NoAFB case in this stage. During the second haze episode (1–4 March), the increases in $PM_{2.5}$ concentration due to aerosol feedback were 25 μg m^{-3}, 45 μg m^{-3} and 24 μg m^{-3}, with the fractional changes of 21%, 35% and 34%, respectively, which are lower than the feedback effect during the first haze episode. So, in terms of magnitude, the largest feedback effect on $PM_{2.5}$ occurred in the persistence stage, followed by that in the growth stage, although the fractional change of $PM_{2.5}$ was larger in the dissipation stage.

Table 5 summarized the average feedback-induced changes in meteorological variables and $PM_{2.5}$ concentrations over the BTH region during the entire and the first haze periods. During the study period, due to the radiative feedback by all aerosols (FULL minus NoAFB), surface air temperature and wind speed decreased by 1.4 °C and 0.04 m s^{-1}, respectively, with RH increased by 8.7% in the BTH. PBL height was reduced by 160 m (or a percentage change of -18.6%) on average, along with a reduction of 3.3 m^2 s^{-1} (-27.0%) in vertical diffusivity coefficient (K_z), resulting in an increase of $PM_{2.5}$ level by 20.0 μg m^{-3} (28.6%). It is noticed that the above changes were strengthened during the severe haze episode on 20–26 February, with the 7-day average decreases in T2, WS10, PBL height and K_z being up to -1.8 °C, -0.5 m s^{-1}, -183.6 m (-31.0%) and 3.9 m^2 s^{-1} (-48.8%), respectively, and the $PM_{2.5}$ concentration increased by 45.1 μg m^{-3} with a percentage increase of 38.7%. Because aerosols affect solar radiation in daytime, in term of daytime mean, the 7-day mean changes in T2, WS10 and PBL height were estimated to be -2.5 °C, -0.6 m s^{-1} and -307.3 m (-37.6%), respectively, leading to an increase of 49.3 μg m^{-3} (48.5%) in $PM_{2.5}$ concentration.

The impact of aerosol radiative feedback in Beijing (Table 6) was stronger than the regional mean. During the first haze episode, the 7-day average changes in T2, WS10, RH2, PBL and $PM_{2.5}$ were estimated to be -2.1 °C, -0.6 m s^{-1}, 17.0%, -195.6 m (-35.9%) and 68.0 μg m^{-3} (39.1%), respectively, and the daytime mean change in $PM_{2.5}$ concentration increased to 83.2 μg m^{-3} (60%), respectively.

Table 7 presents the average changes in major aerosol components (BC, sulfate and nitrate) in $PM_{2.5}$ induced by the feedback effect. Over the BTH region, the feedback caused the average increases in sulfate and nitrate by 5.0 μg m^{-3} (46.4%) and 6.8 μg m^{-3} (37.3%), respectively, for

the entire period, and by up to 12.6 μg m^{-3} (66.9%) and 14.6 μg m^{-3} (40.9%), for the first haze episode. The feedback-induced increases in BC was 0.9 μg m^{-3} (25.1%) and 1.9 μg m^{-3} (32.9%), respectively, for the entire period and the first haze episode. It was noticed that the feedback-induced changes in sulfate and nitrate concentrations were larger than that in BC concentration. This was because that the concentrations of secondary aerosols were increased not only by weakened vertical diffusivity but also by enhanced chemical reactions due to the radiative feedback, which will be discussed in detail in section 5.2.

The above analysis demonstrates a significant impact of aerosol feedback on $PM_{2.5}$ concentration during winter haze episodes in the BTH region. Previous modeling studies reported different degrees of aerosol radiative feedback in east China. Gao et al. (2015) simulated an increase of near surface $PM_{2.5}$ concentrations to be 10-50 μg m^{-3} or 5-25% in the BTH during a severe haze episode on 10-15 January 2013 by using WRF-Chem. For the similar time period and region, Wang et al. (2014a) reported an increase in $PM_{2.5}$ concentrations by 15-50 μg m^{-3} or 10-30% by using a regional coupled model NAQPMS. Wu et al. (2019) used WRF-Chem to investigate a haze episode from 5 December 2015 to 4 January 2016 in the North China Plain and found that the aerosol radiative effects can enhance near-surface $PM_{2.5}$ concentration by 10.2 μg m^{-3} (7.8%) on average.

The results from this study demonstrate a stronger aerosol-radiation feedback than previous modeling studies, with an average increase in $PM_{2.5}$ concentration by up to 45.1 μg m^{-3} (38.7%) during a severe haze episode and further to 49.3 μg m^{-3} (48.5%) for daytime mean over the BTH region. This study also highlights that the aerosol feedback effect can result in an increase of hourly $PM_{2.5}$ concentrations by up to 372 μg m^{-3} (186%) in the vicinity of Shijiazhuang during the severe haze episode. The stronger feedback effect in this study than previous model simulations is mainly due the predicted higher concentration of aerosol components (especially inorganic aerosols) and aerosol optical properties, which are also in a better agreement with observations. It is noticed that a recent study (Zhong et al., 2018a) reported that the aerosol feedback effect contributed over 70% to $PM_{2.5}$ increase during the cumulative explosive stage of haze event in winter Beijing based on integrated analysis of observations from 2013 to 2016, which suggested a dominant role of the feedback effect in haze formation.

5 Process analysis of haze evolution and aerosol radiative feedback

The process analysis (PA) method calculates the Integrated Process Rates (IPRs) and is applied to quantify the individual contributions of different physical and chemical processes to variations of $PM_{2.5}$ and its chemical components. These processes include emission, horizontal and vertical advections (HADV and VADV), horizontal and vertical diffusions (HDIF and VDIF), dry deposition (DDEP), cloud (CLD, including aqueous chemistry and wet scavenging), gas chemistry (GAS), thermodynamic chemistry (Thermo) and heterogeneous chemistry (HET). The focus of this study is Beijing, so the model grid cell near the surface having Beijing is selected for analysis.

5.1 The mechanism of haze evolution related to various processes

5.1.1 Haze evolution during 20–26 February

There was a severe haze event lasting for about 7 days, with the maximum hourly $PM_{2.5}$ up to 482 μg m^{-3} on 26 February. This haze was initially formed on 20 February, with the observed surface $PM_{2.5}$ concentration less than 50 μg m^{-3} on 19 February, rapidly increased to 343 μg m^{-3} on 20 February, and reached 482 μg m^{-3}, followed by rapid haze dissipation on 26 February due to the arrival of a cold front.

PA was used to provide insights into the evolution mechanism of the haze episode, which was divided into the clean, growth, persistence and dissipation stages in this study. Figure 8 shows the average process budgets for changes in $PM_{2.5}$ (which is the sum of sulfate, nitrate, ammonium, BC, OC, SOC and primary $PM_{2.5}$) and its major components in Beijing during the four stages of the first haze period (Figure 8) from the FULL simulation. Figure 8a shows the hourly IPRs of $PM_{2.5}$ by physical and chemical processes. The emission of primary aerosols was the largest contributor to the $PM_{2.5}$ mass with a constant IPR of 29.8 μg m^{-3} h^{-1} (not shown in Figure 8a for clarity) due to the use of a monthly based emission inventory. Chemical processes (GAS, Thermo and HET) also contributed largely to $PM_{2.5}$, with generally larger contributions in the growth and persistence stages. Thermodynamic equilibrium processes and gas chemistry accounted for over 2/3 of the chemical contributions, with the former process

mainly accounting for the formation of nitrate and ammonium and the latter one for sulfate formation. The contribution from heterogeneous reactions was generally small, but when conditions were favorable (such as high RH and high aerosol concentration providing sufficient reaction surfaces), its contribution would also be significant, such as on the morning of 22 February, at nighttime from 23 to 24 February, and on the mornings of 25 and 26 February. Vertical diffusion and dry deposition consistently removed $PM_{2.5}$ from the atmosphere. In general, the larger IPRs from both VDIF and DDEP during the clean and dissipation stages resulted in lower $PM_{2.5}$ concentrations, whereas the lower IPRs from VDIF and DDEP in the growth stage favored aerosol accumulation. In the persistence stage, the IPRs of VDIF and DDEP were generally small. It should be noted that on every midday, when PBL was fully developed, the vertical diffusion reached the daily maximum, producing distinctly large negative IPRs of VDIF. Advections (HADV and VADV) and horizontal diffusion either contributed to the accumulation or loss of $PM_{2.5}$. During this severe haze episode, horizontal diffusion served as a sink of $PM_{2.5}$, producing a negative IPR of HDIF through the event. Horizontal advection served as a sink of $PM_{2.5}$ in most of the time, leading to a negative IPR of HADV, however, when the removal of $PM_{2.5}$ by vertical diffusion was strong at the midday, aerosols were advected to Beijing from surrounding areas due to mass balance, resulting in a positive IPR of HADV. The positive IPR of VADV during the growth and persistence stages of this event indicated that the downward transport of aerosols from upper levels also contributed to the $PM_{2.5}$ increase, such as on the mornings of 22 and 25 February. In general, the IPRs (represented the net effect of all processes, denoted by the red line in Figure 8a) exhibited small positive values from evening to next morning on every day, indicating a gradually increasing $PM_{2.5}$ concentration, whereas on every midday, relatively large negative IPRs occurred, indicating an apparent decrease in $PM_{2.5}$ concentration at that time. It should be mentioned that even in the persistence stage, the diurnal variation of $PM_{2.5}$ occurred although the change rates were generally weaker than those in the growth and dissipation stages.

Figure 8b to 8f show the mean IPRs for $PM_{2.5}$ and its major chemical components as well as the key meteorological variables averaged over each stage to help interpret the formation and evolution mechanism of this severe haze episode.

In the clean stage, emission and chemistry were the two major processes for $PM_{2.5}$

production (Figure 8b). Emission contributed predominately to $PM_{2.5}$ production (IPRs of 29.8 μg m^{-3} h^{-1}), whereas the contributions of gas (9.2 μg m^{-3} h^{-1}) and thermodynamic chemistry (7.3 μg m^{-3} h^{-1}) were comparable. The most influential process for $PM_{2.5}$ removal was vertical diffusion, with the IPRs of -30.3 μg $m^{-3}h^{-1}$, comparable to that of emission. Dry deposition was the second most important process for $PM_{2.5}$ loss (-12.2 μg m^{-3} h^{-1}), followed by horizontal diffusion. Advection had a negligible effect on $PM_{2.5}$ in this stage. In the growth stage, it is noteworthy that the contributions from vertical diffusion (VDIF) and dry deposition (DDEP) to $PM_{2.5}$ removal decreased markedly from -30.3 μg m^{-3} h^{-1} and -12.2 μg m^{-3} h^{-1} in the clean stage to -21.6 μg m^{-3} h^{-1} and -9.2 μg m^{-3} h^{-1}, respectively (Figure 8b), mainly due to the decrease in wind speed and the increase in stability indicated by the reduced vertical diffusivity coefficient K_z (Figure 8f), leading to increases in concentrations of all species. It is impressive that the contributions from chemical processes (GAS+Thermo+HET) increased apparently compared with those in the clean stage, with the IPRs from gas, thermodynamic and heterogeneous chemistry increase to 12.1 μg m^{-3} h^{-1}, 16.0 μg m^{-3} h^{-1} and 5.4 μg m^{-3} h^{-1}, respectively. The increase in the contribution from heterogeneous chemistry was mainly attributed to the increase in relative humidity and aerosol surfaces, upon which heterogeneous reactions took place. It is noticed that the contribution of thermodynamic chemistry increased with increasing relative humidity as well along with haze formation (Figure 8f). The increase in the contribution of thermodynamic chemistry was remarkable (with IPR from 7.3 to 16 μg m^{-3} h^{-1}), because gas precursors of aerosols increased due to weakened vertical diffusivity and higher relative humidity during haze period favored condensation from gas to aerosol phase. It is of interest that vertical advection also contributed to $PM_{2.5}$ production (IPR of 5.4 μg m^{-3} h^{-1}) in this stage, which indicated a potential downward import of $PM_{2.5}$ from upper layer. It is also noticed that horizontal advection contributed to $PM_{2.5}$ loss (-12.8 μg m^{-3} h^{-1}). This is because the strong gradient between the increased $PM_{2.5}$ level in Beijing caused by weakened vertical diffusivity and the relatively lower $PM_{2.5}$ level in the surrounding areas, which led to an outflow of $PM_{2.5}$. In the growth stage, the net variation rate (IPR) of $PM_{2.5}$ concentration was 14.1 μg m^{-3} h^{-1}, in which emissions, chemical processes (GAS+Therm+HET) and physical processes (HADV+VADV+HDIF+VDIF+DDEP) contributed 29.8 μg m^{-3} h^{-1}, 33.5 μg m^{-3} h^{-1} and -49.2 μg m^{-3} h^{-1}, respectively. In the persistence stage, chemical production rate of $PM_{2.5}$

changed slightly, and the production and loss rates of $PM_{2.5}$ were similar, leading to an approximately zero IPR in this stage (Figure 8b). In the dissipation stage, the contribution of vertical diffusion and dry deposition to $PM_{2.5}$ loss increased largely, while the total chemical production rate decreased, which resulted in a net IPR of -34.8 μg m^{-3} h^{-1}, indicating a substantial decrease in $PM_{2.5}$ concentration (Figure 8b). It was also noticed that HADV contributed to $PM_{2.5}$ production in this stage, which was due to mass import to Beijing from upwind areas by northwesterlies.

It should be mentioned that the contribution of emission was unchanged because the monthly based emission inventory from MEIC was used, and the contribution of cloud process was generally negligible throughout the period because there was little cloud and precipitation during the study period.

We further use PA to interpret evolution processes of primary (BC) and secondary (sulfate and nitrate) aerosols.

Black carbon is considered to be inert and chemical inactive, so it is governed solely by physical processes. In the clean stage, BC production was contributed solely by emission (5.7 μg m^{-3} h^{-1}), whereas vertical diffusion and dry deposition contributed equally to BC loss (-2.7 μg m^{-3} h^{-1}), and other processes were negligible (Figure 8c). In the growth stage, the contribution of vertical diffusion and dry deposition to BC loss decreased to -2.0 μg m^{-3} h^{-1} and -1.7 μg m^{-3} h^{-1}, respectively, and the net rate of change was 0.7 μg m^{-3} h^{-1}, indicating a rapid increase of BC concentration in this stage (Figure 8c). In the persistence stage, the loss rate by vertical diffusivity and dry deposition further increased mainly due to the increased BC concentration (Figure 8c). It is noticed that horizontal advection somewhat contributed to the loss of BC (-0.7 μg m^{-3} h^{-1}), which indicated an increasing outflow of BC to surrounding areas. The IPR was near zero, indicating a balance of production and loss rate in this stage. In the dissipation stage, BC loss via vertical diffusion and dry deposition processes increased largely, mainly due to increasing wind speed and vertical diffusivity, and the net IPR became -1.6 μg m^{-3} h^{-1}. This absolute value was larger than that in the growth stage (0.7 μg m^{-3} h^{-1}), which indicated a faster decrease in BC concentration than the BC increase in the growth stage (Figure 8c).

As for secondary aerosols, like sulfate, contribution from direct emission was near zero.

In the clean stage, gas chemistry (5.9 μg m^{-3} h^{-1}) was the predominant process for sulfate production, and vertical diffusion contributed most to the loss (-5.2 μg m^{-3} h^{-1}) (Figure 8d). In the growth stage, contribution from vertical diffusion was reduced to -3.9 μg m^{-3} h^{-1} mainly due to the decreased vertical diffusivity (Figure 8f), whereas positive contribution from gas chemistry increased to 6.6 μg m^{-3} h^{-1}, which was resulted from competitive processes. For sulfate formation from gas chemistry (SO_2+OH→H_2SO_4, followed by nucleation or condensation into particulate phase), the oxidation of SO_2 to sulfate was weakened because of decreasing OH radical due to increasing aerosol attenuation of solar radiation, however, SO_2 increased due to weakened vertical diffusivity, leading to a slight net increase of sulfate concentration compared with the clean stage. It is noteworthy that the sulfate production rate from heterogeneous reactions increased to 2.7 μg m^{-3} h^{-1}, mainly due to the increases in SO_2, aerosol surfaces and RH (as well as aerosol water content). All the processes led to a net sulfate production rate of 2.7 μg m^{-3} h^{-1}, in which chemistry played a predominant role (IPR of 9.3 μg m^{-3} h^{-1}). In the persistence stage, the contribution of gas and heterogeneous processes further increased to 7.4 μg m^{-3} h^{-1} and 4.3 μg m^{-3} h^{-1}, indicating an increasing sulfate production through chemical processes (Figure 8d). It is interesting to note that vertical diffusion contributed more to sulfate loss than in the growth stage, which was mainly due to the higher sulfate level than in the growth stage while vertical diffusivity coefficients were almost the same. The net IPR in this stage was just 0.2 μg m^{-3} h^{-1}, which indicated an approximate balance of production and loss. In the dissipation stage, increasing vertical diffusivity was the dominant process for sulfate loss, and chemical contribution decreased. It is noticed a positive contribution to sulfate from horizontal advection (IPR of 4.3 μg m^{-3} h^{-1}), which was due to an import of sulfate from upwind areas of Beijing by northwesterly winds, like those for $PM_{2.5}$ and BC.

For nitrate, in the clean stage, thermodynamic process (4.5 μg m^{-3} h^{-1}) was the largest contributor to nitrate production (Figure 8e). During the growth stage, the contribution of thermodynamic processes (10.2 μg m^{-3} h^{-1}) increased by over a factor of two and was larger than the contribution from heterogeneous process (Figure 8e). The substantial increase in the contribution of thermodynamic processes to nitrate production was due to the combined effects of the increased level of nitrate precursors (HNO_3 and NH_3) resulting from weakened

diffusivity and the increased RH along with the decreased air temperature, which were favorable for gas to aerosol conversion. The contribution of heterogeneous reactions increased as well due to the increased aerosol surface and relative humidity. The net rate of nitrate change in this stage was 5.3 μg m^{-3} h^{-1}. In the persistence stage, the contribution from heterogeneous reactions changed slightly while the contribution from thermodynamic process somewhat reduced (Figure 8e). This is because more NH_3 was consumed to neutralize the increased sulfate, leaving less NH_3 to react with HNO_3, and thus producing fewer nitrate. The near zero net IPR of nitrate in this stage also indicated a balance of production and loss. In the dissipating stage, the contribution of chemical processes was almost the same as that in the clean stage, while physical processes dominated the loss and the net IPR of nitrate (Figure 8e).

5.1.2 Haze evolution during 1–4 March

We also investigate another haze period of 1–4 March using PA (Figure 9). The hourly IPRs by different processes are shown in Figure 9a. An apparent difference between this episode and the first one was the positive IPRs of HADV during this episode, especially in the growth stage from 21:00 (LST) on 1 March to 9:00 (LST) on 2 March, which indicated that horizontal transport contributed to the haze formation. Another difference is that the chemical processes, especially heterogeneous reactions contributed less to the $PM_{2.5}$ mass during the persistence stage, such as from 10:00 (LST) on 2 March to 3:00 (LST) on 4 March, which will be discussed below.

The IPRs for $PM_{2.5}$ and its components and meteorological variables averaged over each stage during this episode are calculated and presented in Figure 9b to 9f. For BC (Figure 9c), the most evident difference from the first haze episode occurred in the growth stage, in which horizontal advection contributed 1.5 μg m^{-3} h^{-1} to BC production, which was comparable in magnitude to the negative contributions from vertical diffusion and dry deposition (-1.3 μg m^{-3} h^{-1}), suggesting the import of BC into Beijing from surrounding areas. The wind direction in the south of Beijing at this stage was southerly and wind speed was about 2-3 m s^{-1}, so the transport of pollutants from southern Hebei apparently contributed to the increase of BC level in Beijing. Differently, during the first haze event on 20–26 February, wind direction was easterly, bringing less polluted air mass from the Bohai Sea and northern Tianjin, so horizontal

advection contributed less to BC in Beijing. This transport feature was also reflected in the change rates of sulfate (Figure 9d), nitrate (Figure 9e) and $PM_{2.5}$ (Figure 9b) concentrations. An observational study for the same haze period in Beijing (Ma et al., 2017) also suggested the important role of regional transport from the south of Beijing in haze formation.

For sulfate (Figure 9d), although chemical processes still contributed most to sulfate production in the growth stage (6.0 $\mu g\ m^{-3}\ h^{-1}$), it is noticed that gas chemistry (5.9 $\mu g\ m^{-3}\ h^{-1}$) accounted for most of the sulfate production, whereas contribution from heterogeneous reactions was smaller than that in the first haze episode mainly due to lower relative humidity. In the growth stage, the net IPR was 1.9 $\mu g\ m^{-3}\ h^{-1}$, 30% smaller than that for the first haze, indicating a weaker secondary aerosol formation during this haze episode. In the persistence stage, sulfate production from gas phase oxidation was almost balanced by the loss from dry deposition and vertical diffusion, resulting in a net IRP of -0.1 $\mu g\ m^{-3}\ h^{-1}$, indicating a small variation of sulfate concentration during this stage on average.

For nitrate, in the growth stage, it is of interest to note that heterogeneous reactions (5.5 $\mu g\ m^{-3}\ h^{-1}$) dominated over thermodynamic processes (2.7 $\mu g\ m^{-3}\ h^{-1}$) in nitrate formation, which could be due to the low RH in this stage. Fountoukis and Nenes (2007) indicated that nitrate aerosol is hardly formed in the ISORROPIA II model when RH is below 40%. The average RH is about 37% during this haze episode, resulting in more nitrate formed by heterogeneous reactions. The net IPR in the growth stage was 3.7 $\mu g\ m^{-3}\ h^{-1}$, approximately 30% smaller than that in the first haze episode. In the persistence stage when relative humidity increased to 51%, nitrate formation via thermodynamic processes became important, and due to competition, nitrate formation from heterogeneous reactions was reduced.

For $PM_{2.5}$ (Figure 9b), in the growth stage, the IPR of $PM_{2.5}$ concentration was 13.0 $\mu g\ m^{-3}\ h^{-1}$, in which emission, chemical processes (GAS+Therm+HET) and physical processes (HADV+VADV+HDIF+VDIF+DDEP) contributed 29.8 $\mu g\ m^{-3}\ h^{-1}$, 23.9 $\mu g\ m^{-3}\ h^{-1}$ and -40.7 $\mu g\ m^{-3}\ h^{-1}$, respectively. It is noteworthy that horizontal advection process (HADV) contributed 22.4 $\mu g\ m^{-3}\ h^{-1}$ to $PM_{2.5}$ production in this episode, which was comparable to the total chemical production of 23.9 $\mu g\ m^{-3}\ h^{-1}$. This reveals the comparable contributions to $PM_{2.5}$ in Beijing from local sources and regional transport during this haze episode. In the persistence stage, because of the change in wind direction and lower wind speed, the regional transport of $PM_{2.5}$

became weak. The IPRs were -4.0 μg m^{-3} h^{-1} for HADV and 1.2 μg m^{-3} h^{-1} for VADV, respectively, which were obviously smaller than those in the first haze episode. In the dissipation stage, physical processes except HADV all contributed to the loss of $PM_{2.5}$. Compared with the first haze episode, the negative IPR of VADV decreased mainly due to the larger wind speeds in this episode, as more $PM_{2.5}$ was removed by VADV, the remaining $PM_{2.5}$ loss by vertical diffusion decreased, consequently a weakened VDIF. The positive IPR of HADV increased as well due to larger wind speed than that in the first episode in this stage.

The above process analyses reveal that for the first haze episode (20–26 February) in Beijing, local emissions and chemical processes were the main contributors to the formation and persistence of the haze event. However, for the second haze (1–4 March), regional transport or horizontal advection played a more important role in haze formation, with a similar magnitude to local emissions and chemical productions in the growth stage. In all, for both episodes, local emission, chemical reaction and horizontal advection were major processes contributing to $PM_{2.5}$ increase, whereas vertical processes (diffusion, dry deposition and advection) were major processes for $PM_{2.5}$ removal. As the pollution level increased, the contribution of secondary aerosols through chemical formation to $PM_{2.5}$ increased apparently in Beijing.

5.2 Contributions of physical and chemical processes to the aerosol feedback

5.2.1 The first haze episode (20–26 February)

Figure 10 shows the contributions of each process to the feedback-induced difference in the change rates of $PM_{2.5}$ and its major components (ΔIPR) during the first haze episode (20–26 February), which were derived from the difference between cases with and without aerosol radiative effects (FULL minus NoAFB).

The definition of the four stages during haze evolution is the same as that in section 5.1.1. For BC (Figure 10b) in the clean stage, the aerosol feedback caused a decrease in vertical diffusion and advection (Figure 10e), leading to an increase in BC concentration with the ΔIPR of 0.40 μg m^{-3} h^{-1} from VDIF+VADV, concurrently, the feedback caused an increased loss of BC through horizontal diffusion (HDIF) and advection (HADV) and dry deposition (DDEP) due to the increased BC concentration, with the ΔIPR of -0.39 μg m^{-3} h^{-1} from

HADV+HDIF+DDEP (Figure 10b). The net ΔIPR was near zero, which indicated a negligible feedback effect during the clean stage. In the growth stage, the feedback caused a pronounced decrease in vertical diffusivity, advection, as well as dry deposition velocity, leading to apparent increases in BC level, with the contributions to ΔIPRs from VDIF, VADV, and DDEP being 0.50 $\mu g\ m^{-3}\ h^{-1}$, 0.50 $\mu g\ m^{-3}\ h^{-1}$ and 0.20 $\mu g\ m^{-3}\ h^{-1}$, respectively (Figure 10b). The increase in BC concentration consequently led to an increase in outflow via HADV and HDIF, with the ΔIPRs of -0.63 $\mu g\ m^{-3}\ h^{-1}$ and -0.12 $\mu g\ m^{-3}\ h^{-1}$, respectively, which tended to reduce BC concentration. The total effect by summing the processes exhibited a net positive ΔIPR of 0.44 $\mu g\ m^{-3}\ h^{-1}$, which indicated an apparent increase in BC concentration due to the feedback. In the persistence stage, the sign of ΔIPR for each process was the same as that in the growth stage, and the ΔIPR by vertical processes (0.84 $\mu g\ m^{-3}\ h^{-1}$ from VADV+VDIF+DDEP) was generally balanced by that of horizontal processes (-0.80 $\mu g\ m^{-3}\ h^{-1}$ from HADV+HDIF) and led to a net ΔIPR of 0.04 $\mu g\ m^{-3}\ h^{-1}$ (Figure 10b), which indicated the difference in the BC change rate between the FULL and NoAFB cases was small in this stage. In the dissipating stage, the ΔIPRs were negative for all the processes except for HADV. This was because of the higher BC levels due to the feedback, which caused more BC to be removed than without feedback, although the vertical diffusion coefficient was smaller due to the feedback. The positive ΔIPR from HADV suggested the enhanced BC import into Beijing from upwind regions due to the feedback. The sum of these processes produced a net ΔIPR of -1.20 $\mu g\ m^{-3}\ h^{-1}$, which indicated a larger decreasing rate of BC concentration (from haze to clean level) due to aerosol feedback in this stage.

For sulfate (Figure 10c), in the clean stage, the feedback-induced changes were as small as those for BC. In the growth stage, besides the positive ΔIPRs by VDIF, VADV and DDEP as those for BC, the most impressive feature was the larger contributions from GAS and HET, with the ΔIPRs being 0.29 $\mu g\ m^{-3}\ h^{-1}$ and 1.73 $\mu g\ m^{-3}\ h^{-1}$, respectively, much larger than those (0.11 $\mu g\ m^{-3}\ h^{-1}$ and 0.23 $\mu g\ m^{-3}\ h^{-1}$) in the clean stage because of the increased gas precursors, aerosol surfaces and RH due to the feedback effect, which enhanced chemical formation (Figure 10c, 10e). The sum of the ΔIPRs by all the processes was 1.92 $\mu g\ m^{-3}\ h^{-1}$, indicating an apparent increase in sulfate concentration due to the feedback effect. In the persistence stage, the ΔIPRs by GAS and HET increased. However, the ΔIPR of VDIF became negative, which

could be explained by the increased sulfate concentration due to aerosol feedback caused more sulfate to be removed through vertical diffusion, leading to a negative ΔIPR of VDIF, although the vertical diffusion coefficient was reduced by the feedback. In the dissipation stage, the ΔIPR by HET decreased because the feedback-induced differences in the concentrations of precursors and aerosols became smaller. The large negative ΔIPR by VDIF indicated a larger decreasing rate in sulfate concentration from the persistence to clean stages due to the feedback.

For nitrate (Figure 10d), the feedback-induced IPR changes in the clean stage were similar to those for sulfate. In the growth stage, remarkable increases in nitrate formation from Thermo and HET processes occurred, with the ΔIPRs of 3.30 $\mu g\ m^{-3}\ h^{-1}$ and 0.50 $\mu g\ m^{-3}\ h^{-1}$, respectively (Figure 10d). The increased gas precursors and RH due to the aerosol feedback reinforced chemical formation processes. In this stage, the overall ΔIPR was 3.90 $\mu g\ m^{-3}\ h^{-1}$, suggesting a faster increasing rate in nitrate concentration in consideration of aerosol feedback. In the persistence stage, the ΔIPR by Thermo was smaller than that in the growth stage (Figure 10d). This could be explained that the apparent increase in sulfate concentration via HET and GAS due to the feedback (Figure 10c) in this stage consumed more ammonia, which inhibited the formation of nitrate ammonium via thermodynamic processes. The net ΔIPR by all the processes in this stage was near zero, which indicated that the radiative feedback exerted little effect on the change rate of nitrate concentration during this stage. In the dissipation stage, the attenuation of solar radiation by aerosols was weakened because of the decrease in aerosol concentration, meanwhile, the concentrations of gas precursors (NO_x) were elevated due to the feedback, the combined effect resulted in an increase of photochemical production of HNO_3; in addition, RH was increased due to the feedback as well, as a result, nitrate formation via thermodynamic process was enhanced, leading to a positive ΔIPR of 3.73 $\mu g\ m^{-3}\ h^{-1}$ by Thermo in this stage.

For $PM_{2.5}$, the net ΔIPR due to aerosol feedback in the clean stage was 0.30 $\mu g\ m^{-3}\ h^{-1}$, in which 1.22 $\mu g\ m^{-3}\ h^{-1}$ was from chemical processes (GAS+Thermo+HET) and -0.90 $\mu g\ m^{-3}\ h^{-1}$ from physical processes (HADV+VADV+HDIF+VDIF+DDEP) (Figure 10a). In the growth stage, the net ΔIPR was 9.50 $\mu g\ m^{-3}\ h^{-1}$, which meant in every hour, approximate 9.50 $\mu g\ m^{-3}$ of $PM_{2.5}$ mass was elevated in Beijing due to the feedback effect. The above feedback-induced difference in the change rate of $PM_{2.5}$ (ΔIPR) resulted from a combined effect from chemical

processes (7.27 μg m^{-3} h^{-1}) and physical processes (2.23 μg m^{-3} h^{-1}), which suggested that chemical processes contributed more to the $PM_{2.5}$ increase than physical processes. However, it was noted that the increased contribution from chemical processes was related to increasing gas precursors, which was partly associated with physical processes. It was noteworthy that the positive ΔIPRs were contributed by both chemical processes (GAS, Thermo and HET) and vertical movements (VADV, VDIF and DDEP) (Figure 10a). The sum of positive ΔIPRs was 22.88 μg m^{-3} h^{-1}, in which 7.27 μg m^{-3} h^{-1} was from chemical processes and 15.61 μg m^{-3} h^{-1} from vertical movements. This suggested a larger feedback-induced $PM_{2.5}$ increase through vertical movements than via chemical processes. However, the outflow (HADV+HDIF) of $PM_{2.5}$ was also enhanced due to the increased $PM_{2.5}$ level by aerosol feedback, producing a negative ΔIPR (-13.38 μg m^{-3} h^{-1}), and partly offsetting the positive ΔIPR (15.61 μg m^{-3} h^{-1}) by vertical movements, resulting in a net ΔIPR of 2.23 μg m^{-3} h^{-1} from all the physical processes. In the persistence stage, the sign of ΔIPRs by different processes generally resembled those in the growth stage except that of VDIF whose ΔIPR was negative, which indicated more removal though VDIF mainly due to the increased secondary aerosol concentrations by aerosol feedback. The net ΔIPR by all the processes was 0.40 μg m^{-3} h^{-1} in this stage, indicating a small influence of aerosol feedback on the change rate of $PM_{2.5}$ concentration. In the dissipating stage (Figure 10a), the large negative ΔIPR from VDIF indicated more $PM_{2.5}$ mass was removed via vertical diffusion while considering aerosol feedback, although the feedback induced a smaller vertical diffusivity coefficient. The net ΔIPR of -24.60 μg m^{-3} h^{-1} indicated a larger decreasing rate of $PM_{2.5}$ concentration in the FULL case than in the NoAFB case.

5.2.2 The second haze episode (1–4 March)

For BC in the second haze episode (1–4 March), the most obvious difference from the first episode was in the growth stage, in which the ΔIPR by horizontal advection (HADV) was 0.70 μg m^{-3} h^{-1} (Figure 11b). The radiative feedback led to a weakened vertical diffusivity and a decreased PBL height (Figure 11e), which favored the accumulation of BC and caused a positive ΔIPR of 0.40 μg m^{-3} h^{-1} from VDIF. The wind direction in the growth stage was southerlies as discussed above, bringing aerosols from the south to Beijing. The aerosol feedback enhanced BC concentration in source regions through reducing vertical diffusivity,

leading to an increased northward flux of BC and a positive ΔIPR from HADV. The higher BC concentration due to the feedback via HADV and VDIF consequently led to an increase in BC outflow out of Beijing via vertical advection (VADV) and horizontal diffusion (HDIF), with the ΔIPRs of -0.60 μg m^{-3} h^{-1} and -0.20 μg m^{-3} h^{-1}, respectively. In this stage, the net ΔIPR of BC was 0.20 μg m^{-3} h^{-1}, in which 0.50 μg m^{-3} h^{-1} was from horizontal movements (HADV+HDIF) and -0.30 μg m^{-3} h^{-1} from vertical movements (VADV+VDIF+DDEP), indicating that the feedback effect strengthened the contribution of horizontal movements to surface BC concentration in Beijing. In the persistence stage (Figure 11b), the net ΔIPR was also near zero (-0.02 μg m^{-3} h^{-1}), indicating that the BC change rate was merely affected by the feedback in this stage. In the dissipation stage (Figure 11b), the ΔIPRs were negative for all the processes except for VDIF. This could be attributed to the higher BC levels due to the feedback, which caused more BC to be removed than without feedback through these processes. The net ΔIPR was -0.17 μg m^{-3} h^{-1}, the same as that in the growth stage, but with opposite sign.

For sulfate (Figure 11c), in the growth stage, different from the relatively large positive ΔIPR by chemical processes in the first haze episode, the feedback caused small IPR changes via chemical production because SO_2 concentration in this episode was lower than that in the first one and sulfate was mainly formed in upwind regions and transported to Beijing. Consequently, relatively large sulfate increases through HADV and VDIF in this episode. In this stage, the feedback caused a slight increase in sulfate concentration by GAS with ΔIPR of 0.17 μg m^{-3} h^{-1} due to slightly elevated precursors, however, because of the low relative humidity (mean RH was 38%) and competitive processes, heterogeneous reactions were depressed. In terms of physical processes, due to the feedback effect, horizontal transport (HADV) was strengthened (ΔIPR of 1.0 μg m^{-3} h^{-1}) due to the increased sulfate concentration to the south of Beijing, meanwhile, the weakened vertical diffusivity caused an increase in sulfate concentration by VDIF and DDEP, with the ΔIPRs of 1.0 μg m^{-3} h^{-1} and 0.57 μg m^{-3} h^{-1}, respectively, consequently, the outflow of sulfate out of Beijing was also increased via vertical advection (VADV) and horizontal diffusion (HDIF). The net ΔIPR in the growth stage was 0.90 μg m^{-3} h^{-1}, indicating an apparent increase in sulfate concentration due to the feedback. In the persistence stage, the ΔIPRs by GAS and HET changed slightly compared with those in the growth stage. The negative ΔIPR by VDIF indicated more loss of sulfate by vertical

diffusion while considering aerosol feedback. The net ΔIPR in this stage was 0.02 μg m^{-3} h^{-1}, indicating a negligible feedback effect on sulfate change rate in this stage. In the dissipation stage, the feedback-induced higher sulfate concentration caused more removal of sulfate via physical processes except HADV, resulting in a net ΔIPR of -0.64 μg m^{-3} h^{-1}. The positive ΔIPR from HADV was due to the strengthened import from upwind areas due to the feedback.

For nitrate, in the growth stage, the feedback also induced an increase in nitrate concentration via horizontal advection like sulfate (Figure 11d). The increases in gas precursors and aerosol surfaces due to the feedback enhanced nitrate formation, resulting in nitrate increases via Thermo and HET, with the ΔIPRs of 0.88 μg m^{-3} h^{-1} and 0.46 μg m^{-3} h^{-1}, respectively. To the persistence stage, the chemical production of nitrate increased largely caused by the feedback, with the ΔIPR of Thermo being 4.30 μg m^{-3} h^{-1}. The reason could be the low RH in the growth stage (38% shown in Figure 9f) left most of nitric acid remained in gas phase together with the increase in RH due to the feedback (13.2% shown in Figure 11e) drove its conversion from gas to aerosol phase. Due to the enhanced thermodynamics production, nitrate formation via heterogeneous reactions was depressed in this stage. The increased nitrate concentration via Thermo led to larger removal via vertical diffusion, resulting in a negative ΔIPR of -4.80 μg m^{-3} h^{-1} by VDIF, and a net ΔIPR of -0.10 μg m^{-3} h^{-1}. In the dissipation stage, like that in the first haze episode, the reduced aerosol attenuation of solar radiation and increased RH induced by aerosol feedback led to an increase in nitrate via thermodynamic process, with the ΔIPR of 1.80 μg m^{-3} h^{-1} by Thermo. Consequently, heterogeneous reactions were depressed due to competitive processes (ΔIPR of -0.97 μg m^{-3} h^{-1} by HET). In this stage, because of the higher nitrate concentration, the feedback led to larger removal by vertical processes (the ΔIPR of VADV+VDIF+DDEP was -3.23 μg m^{-3} h^{-1}), with a net ΔIPR of -1.78 μg m^{-3} h^{-1}, similar to the ΔIPR in the growth stage but with opposite sign.

For $PM_{2.5}$ (Figure 11a), the net ΔIPR due to aerosol feedback in the growth stage was 2.40 μg m^{-3} h^{-1}, with 1.40 μg m^{-3} h^{-1} from physical processes (HADV+VADV+HDIF+VDIF+DDEP) and 1.0 μg m^{-3} h^{-1} from chemical processes (GAS+Thermo+HET), which indicated that the feedback-induced increase in $PM_{2.5}$ concentration per hour was produced through larger contributions from physical processes than chemical processes in this episode. HADV contributed most to the $PM_{2.5}$ increase (with ΔIPR of 10.20 μg m^{-3} h^{-1}), followed by VDIF

(with ΔIPR of 2.90 μg m^{-3} h^{-1}). As mentioned above, the weakened vertical diffusivity caused by the feedback enhanced aerosol concentrations in the entire BTH region, meanwhile, the feedback induced a southeast wind anomaly with a slight change in wind speed in the regions south of Beijing. The combined effect of the elevated aerosol concentrations and southeast wind anomaly brought more aerosols to Beijing. In the persistence stage, the feedback increased $PM_{2.5}$ concentration mainly through chemical processes, with the ΔIPR of 6.05 μg m^{-3} h^{-1}, which was mainly resulted from the enhanced thermodynamic production of ammonium nitrate, and such increase in aerosol mass due to feedback led to more aerosols to be diffused than that without feedback, leading to the ΔIPR of -7.30 μg m^{-3} h^{-1} by VDIF. It is noticed that the signs of the ΔIPRs by VDIF were opposite between the growth and persistence stages even though the vertical diffusivities were both decreased. In the growth stage, the $PM_{2.5}$ concentration was gradually increasing, the effect of the weakened vertical diffusivity was dominated, resulting in a positive ΔIPR by VDIF which favored further accumulation of aerosols; in the persistence stage, the aerosol concentration had already been elevated to a high level, the effect of higher concentration surpassed that of weakened vertical diffusivity due to the feedback and led to a negative ΔIPR, which meant the feedback caused more loss of $PM_{2.5}$ via VDIF. In the persistence stage, the net ΔIPR was 0.44 μg m^{-3} h^{-1}, in which -5.6 μg m^{-3} h^{-1} from physical processes and 6.05 μg m^{-3} h^{-1} from chemical processes, which indicated the feedback-induced overall changes in the change rate of $PM_{2.5}$ concentration in this stage were relatively small. In the dissipating stage, the removal of $PM_{2.5}$ was enhanced by the feedback through all the processes except HADV mainly due to the increased $PM_{2.5}$ concentration, the positive ΔIPR by HADV was caused by the enhanced import from upwind areas due to the feedback. In this stage, the feedback effect enhanced the removal of $PM_{2.5}$, which was reflected by the net negative ΔIPR of -4.30 μg m^{-3} h^{-1}.

The above analyses quantify the key processes contributing to the aerosol radiative feedback in Beijing during the two haze episodes. In the growth stage of the first haze episode, the feedback-induced $PM_{2.5}$ enhancement was attributed to the positive contributions from chemical processes and vertical movements, but partly offset by the increased outflow of $PM_{2.5}$ via horizontal advection, resulting in a larger increase in $PM_{2.5}$ through chemical processes than that from physical processes. Differently, duirng the second haze episode, the feedback-

induced $PM_{2.5}$ enhancement in the growth stage was larger by physical processes than that by chemical processes, and horizontal advection contributed most to the $PM_{2.5}$ enhancement. In all, the radiative feedback increased the cumulative rate of aerosols in the growth stage via promoting chemical formations, weakening vertical diffusions and/or enhancing regional transport by horizontal advection. For both episodes, the radiative feedback exerted small effect on the change rate of $PM_{2.5}$ concentration during the persistence stage and reinforced the decreasing rate of $PM_{2.5}$ in the dissipation stage.

6 Conclusions

Several severe haze events occurred in the winter of 2014, with the most severe one on 20–26 February. An online-coupled regional atmospheric chemistry/aerosol-climate model (RIEMS-Chem) was developed and utilized to investigate the mechanisms of haze formation and aerosol radiative feedback in the Beijing-Tianjin-Hebei (BTH) region. Two numerical experimentswere conducted to explore the aerosol radiative effects (AREs) and feedbacks on meteorological fields and aerosol distributions. Processes analysis technique was implemented in RIEMS-Chem to quantify the individual contributions from various physical and chemical processes to aerosol evolution and radiative feedback. Model performance was comprehensively evaluated by comparing with a variety of observations for meteorological variables, surface shortwave radiation, PBL heights, $PM_{2.5}$ and its chemical components, as well as aerosol optical properties in the BTH region. The comparisons demonstrated that RIEMS-Chem was able to represent the magnitudes and variations of the above variables reasonably well, in particular, improving the simulation of inorganic aerosols and AOD, which was often underpredicted in current on-line coupled models. It is encouraging that by considering the aerosol radiative effects, the model apparently improved predictions for meteorological variables, $PM_{2.5}$ and its chemical compositions and aerosol optical properties in the BTH region, suggesting the importance and necessity for developing chemistry-climate online coupled models in both air quality and climate research.

During the study period, the meteorological conditions were characterized by weak southerly winds, high RH and low PBL height, which favored aerosol accumulation and haze

formation in the BTH region. The average T2, WS10, RH2, PBL height and $PM_{2.5}$ concentration from the FULL case were simulated to be 0.6 °C, 1.2 m s^{-1}, 67.0%, 698.4 m and 90.0 μg m^{-3}, respectively, over the BTH region during the study period.

The distribution pattern of AOD generally resembled that of $PM_{2.5}$, with the domain mean value of 0.78 and the maximum up to 1.1 during the study period. It was noteworthy that the simulated SSA averaged over the BTH region and the study period was 0.91, which indicated the dominance of scattering aerosols. The domain and period average AREs at the surface, in the atmosphere and at the TOA were estimated to be -37 W m^{-2}, 19 W m^{-2} and -18 W m^{-2}, respectively, and they were enhanced to -57 W m^{-2}, 25 W m^{-2} and -32 W m^{-2} during the most severe haze episode (20–26 February). It was striking that the maximum hourly AREs at the surface and at TOA reached -384 W m^{-2} and -231 W m^{-2} around noon time in the vicinity of Shijiazhuang during the first haze episode. The magnitude of the model simulated AREs during the haze episode in this study agreed favorably with previous observational based estimates.

The aerosol radiative effects generally led to a reduction in surface air temperature in the entire domain with larger decrease in southern BTH (-1.2 °C to -2 °C), accompanied by an increase in RH2 (10% to 16%) and a decrease in PBL height (-240 m to -210 m). The changes in these meteorological variables were strengthened during the severe haze episode. Noticeably, $PM_{2.5}$ concentrations were consistently increased over the BTH region due to the aerosol feedback, with the maximum average increase exceeding 33 μg m^{-3} (33%) in southern Hebei and portions of Beijing and Tianjin during the study period, and the maximum hourly increase was up to 372 μg m^{-3} (186%) in the vicinity of Shijiazhuang during the severe haze episode. In terms of domain and period average, the feedback-induced changes were -1.4 °C for T2, -0.04 m s^{-1} for WS10, 8.7% for RH2, -3.3 m^2 s^{-1} for vertical diffusion coefficient, -160.0 m (-19%) for PBL height and 20.0 μg m^{-3} (29%) for $PM_{2.5}$ concentration. The magnitude of the above changes were enhanced during the severe haze episode, with the 7-day mean changes in T2, WS10, RH2, PBL height and $PM_{2.5}$ concentration being -1.8 °C, -0.5 m s^{-1}, 9.8%, -183.6 m (-31%) and 45.1 μg m^{-3} (39%), respectively, which demonstrated the significant aerosol radiative feedback on $PM_{2.5}$ accumulation and haze formation. The changes in sulfate and nitrate concentrations were larger than that in BC concentration because secondary aerosols were increased not only by weakened vertical diffusivity but also by enhanced chemical reactions

caused by the feedback.

The magnitude of the feedback effect varied remarkably during haze evolution. The absolute change in $PM_{2.5}$ concentration caused by the feedback was largest in the persistence stage, followed by those in the growth stage and in the dissipating stage. In Beijing, the feedback-induced increases in $PM_{2.5}$ concentration were 55 μg m^{-3}, 84 μg m^{-3}, 40 μg m^{-3}, respectively, during the growth, persistence and dissipation stages of the severe haze episode.

PA method was applied to calculate the IPRs for quantifying the individual contributions from physical and chemical processes to variations of $PM_{2.5}$ and its chemical components during haze episodes in Beijing. Two haze episodes were analyzed and compared to elucidate the mechanism of haze formation and evolution. For the first haze episode, the net IPR for $PM_{2.5}$ was 14.1 μg m^{-3} h^{-1} in the growth stage, in which emissions, chemical processes and physical processes contributed 29.8 μg m^{-3} h^{-1}, 33.5 μg m^{-3} h^{-1} and -49.2 μg m^{-3} h^{-1}, respectively, which indicated a remarkable $PM_{2.5}$ increase contributed by chemical processes in this stage. The most influential processes for $PM_{2.5}$ loss and production were vertical diffusion and thermodynamic processes, respectively. Compared with the clean stage, the losses by vertical diffusion and dry deposition reduced largely, and the production by chemical processes increased, both leading to an evident increase in surface $PM_{2.5}$ concentrations in the growth stage. In the persistence stage, the production and loss of $PM_{2.5}$ were almost equal, resulting in an approximately zero IPR in this stage. In the dissipation stage, the loss of $PM_{2.5}$ by vertical diffusion and dry deposition increased greatly, leading to a net IPR rate of -34.8 μg m^{-3} h^{-1}, which meant a substantial decrease in $PM_{2.5}$ concentration.

For the second haze episode, the net IPR for $PM_{2.5}$ was 13.0 μg m^{-3} h^{-1} in the growth stage, in which emissions, chemical processes and physical processes contributed 29.8 μg m^{-3} h^{-1}, 23.9 μg m^{-3} h^{-1} and -40.8 μg m^{-3} h^{-1}, respectively. It was noteworthy that the contribution of horizontal advection to $PM_{2.5}$ was of a similar magnitude to the contributions from local emissions and chemical processes, with the mean IPR of 22.4 μg m^{-3} h^{-1}, which indicated the important contribution of regional transport to haze formation in Beijing. Process analysis for the changes in $PM_{2.5}$ components during haze evolution was also conducted.

The contribution of each physical and chemical process to the feedback-induced changes in $PM_{2.5}$ and its major components were explored and quantified. For the first haze episode,

the fast increase in $PM_{2.5}$ (ΔIPR of 9.5 μg m^{-3} h^{-1}) due to aerosol feedback in the growth stage was mainly attributed to the changes in vertical movements (VDIF and VADV) and chemical processes, but the increased outflow via horizontal advection (HADV) partly offset the increased $PM_{2.5}$ due to vertical movements, which caused a larger contribution to the $PM_{2.5}$ increase from chemical processes (ΔIPR of 7.27 μg m^{-3} h^{-1}) than that from physical processes (ΔIPR 2.23 μg m^{-3} h^{-1}). However, during the second haze episode, the feedback-induced $PM_{2.5}$ increase (ΔIPR of 2.4 μg m^{-3} h^{-1}) in the growth stage was mainly contributed by physical processes (ΔIPR of 1.40 μg m^{-3} h^{-1}) rather than that by chemical processes (ΔIPR of 1.0 μg m^{-3} h^{-1}), and among physical processes, the $PM_{2.5}$ increase was mainly attributed to the increased horizontal advection (ΔIPR of 10.2 μg m^{-3} h^{-1}). In general, in the growth stage of haze episodes, the feedback increased the accumulation rate of aerosols mainly through enhancing chemical formations, weakening vertical diffusions and/or enhancing regional transport by advections. The feedback-induced changes in the change rate of $PM_{2.5}$ concentration were small during the persistence stage, and the feedback enhanced the removal rate of $PM_{2.5}$ in the dissipation stage mainly through increasing vertical diffusion and/or vertical advection.

The results from this study demonstrated a significant impact of aerosol radiative feedback on meteorology, chemistry, aerosol distribution and evolution during winter haze events in the BTH region. The mechanism and processes through which the feedback affected haze formation and evolution were elucidated and quantified. This study is still subject to some uncertainties: 1.) An internal mixing was assumed for aerosol mixing in this study, but the mixing state of aerosols is always changing, while this assumption is generally realistic for haze days, it may overestimate the feedback effect for clean days. 2.) A typical size distribution measured during haze days was used, whereas the size of aerosol internal mixture could change to some extent with aging processes. These uncertainties require further development of model treatment for evolution of aerosol mixing state and size distribution, which is poorly represented in current online coupled models. 3.) Direct aerosol radiative effect dominated the feedback effect in this study, so more cases in different regions and seasons~~,~~ when indirect effect could be more important are needed to elucidate the complete feedback mechanism at different spatial and temporal scales. 4.) Finer model grid resolution is expected to be applied to look into details of the feedback effect at urban scale along with finer emission inventory

(Tao et al., 2020), vertical observations (Wilcox et al., 2016; Wang et al., 2018) and higher computational efficiency when available in the future. Finally, this study pointed out the significance and necessity of developing online coupled model for exploring chemistry/aerosol-weather/climate interactions and for improving meteorological and chemical predictions in both air quality and climate research in the future.

Author Contributions

ZH designed the study, JL performed the model simulation, JL and ZH processed and analyzed the modeling data, ZH and JL wrote the paper, JL and ZX contributed to the model development, YW provided and analyzed the chemical observation data, XX provided the meteorological sounding and aerosol optical observation data, JL and LL processed and analyzed the observational data, RZ synthesized and analyzed the observation.

Data availability.

The observational data can be accessed through contacting the corresponding authors.

Competing interests.

The authors declare that they have no conflict of interests.

Special issue statement.

This article is part of the special issue "Regional assessment of air pollution and climate change over East and Southeast Asia: results from MICS-Asia Phase III". It is not associated with a conference.

Acknowledgement.

This study was supported by the National Natural Science Foundation of China (no. 91644217), the National Key R&D Program of China (2019YFA0606802) and the Jiangsu Collaborative Innovation Center for Climate Change.

References

Albrecht, B.: Aerosols, cloud microphysics, and fractional cloudiness, Science, 245, 1227, https://doi.org/10.1126/science.245.4923.1227, 1989.

An, Z., Huang, R., Zhang, R., Tie, X., Li, G., Cao, J., Zhou, W., Shi, Z., Han, Y., Gu, Z., and Ji, Y.: Severe haze in northern China: A synergy of anthropogenic emissions and atmospheric

processes, P. Natl. Acad. Sci. USA, 116,18, 8657–8666, 2019.
Baklanov, A., Schlunzen, K., Suppan, P., Baldasano, J., Brunner, D., Aksoyoglu, S., Carmichael, G., Douros, J., Flemming, J., Forkel, R., Galmarini, S., Gauss, M., Grell, G., Hirtl, M., Joffre, S., Jorba, O., Kaas, E., Kaasik, M., Kallos, G., Kong, X., Korsholm, U., Kurganskiy, A., Kushta, J., Lohmann, U., Mahura, A., Manders-Groot, A., Murizi, A., Moussiopoulos, N., Rao, S.T., Savage, N., Seigneur, C., Sokhi, R.S., Solazzo, E., Solomos, S., Sorenson, B., Tsegas, G., Vignati, E., Vogel, B., and Zhang, Y.: Online coupled regional meteorology chemistry models in Europe: current status and prospects, Atmos. Chem. Phys., 14, 317-398, doi:10.5194/acp-14-317-2014, 2014.
Beheng, K. D.: A parameterization of warm cloud microphysical conversion processes, Atmos. Res., 33, 193–206, 1994.
Cai, W., Li, K., Liao, H., Wang, H., and Wu, L.: Weather conditions conducive to Beijing severe haze more frequent under climate change, Nature Clim. Change, 7, 257–262, doi: 10.1038/nclimate3249, 2017.
Carslaw, K. S., Boucher, O., Spracklen, D. V., Mann, G. W., Rae, J. G. L., Woodward, S., and Kulmala, M.: A review of natural aerosol interactions and feedbacks within the Earth system, Atmos. Chem. Phys., 10, 1701–1737, doi:10.5194/acp-10-1701-2010, 2010.
Chan, C. and Yao, X.: Air pollution in megacities in China, Atmos. Environ., 42, 1-42, 2008.
Che H., Xia, X., Zhu, J., Li, Z., Dubovik, O., Holben, B., Goloub, P., Chen, H., Estelles, V., Cuevas-Agulló, E., Blarel, L., Wang, H., Zhao, H., Zhang, X., Wang, Y., Sun, J., Tao, R., Zhang, X., and Shi, G.: Column aerosol optical properties and aerosol radiative forcing during a serious haze-fog month over North China Plain in 2013 based on ground-based sunphotometer measurements, Atmos. Chem. Phys., 14, 2125–2138, doi:10.5194/acp-14-2125-2014, 2014.
Chen, L., Zhu, J., Liao, H., Gao, Y., Qiu, Y., Zhang, M. G., Liu, Z. R., Li, N., and Wang, Y. S.: Assessing the formation and evolution mechanisms of severe haze pollution in the Beijing–Tianjin–Hebei region using process analysis, Atmos. Chem. Phys., 19, 10845–10864, 2019.
Cheng, Y., Zheng, G., Wei, C., Mu, Q., Zheng, Bo., Wang, Z., Gao, M., Zhang, Q., He, K., Carmichael, G., Pösch, U., and Su, H.: Reactive nitrogen chemistry in aerosol water as a source of sulfate during haze events in China, Sci. Adv., 2, e1601530, 2016.
Dawson, J. P., Adams, P. J., and Pandis, S. N.: Sensitivity of $PM_{2.5}$ to climate in the Eastern US: a modeling case study, Atmos. Chem. Phys., 7, 4295–4309, 2007.
Dickinson, R.E., Henderson-Sellers, A., and Kennedy, P.J.: Biosphere-Atmosphere Transfer Scheme (BATS) Version 1e as coupled to NCAR Community Climate Model, NCAR Technical Note, NCAR/TN-387+STR, p.72, 1993.
Ding, A., Huang, X., Nie, W., Sun, J., Kerminen, V. M., Petäjä, T., Su, H., Cheng, Y., Yang, X., Wang, M., Chi, X., Wang, J., Virkkula, A., Guo, W., Yuan, J., Wang, S., Zhang, R., Wu, Y., Song, Y., Zhu, T., Zilitinkevich, S., Kulmala, M., and Fu, C.: Enhanced haze pollution by black carbon in megacities in China, Geophys. Res. Lett., 43, 2873-2879, 10.1002/2016gl067745, 2016.
Emmons, L. K., Walters, S., Hess, P. G., Lamarque, J. F., Pfister, G. G., Fillmore, D., Granier, C., Guenther, A., Kinnison, D., Laepple, T., Orlando, J., Tie, X., Tyndall, G., Wiedinmyer, C., Baughcum, S. L., and Kloster, S.: Description and evaluation of the Model for Ozone

and Related chemical Tracers, version 4 (MOZART-4), Geosci. Model. Dev., 3, 43-67, doi:10.5194/gmd-3-43-2010, 2010.

Forkel, R., Werhahn, J., Hansen, A. B., McKeen, S., Peckham, S., Grell, G., and Suppan, P.: Effect of aerosol–radiation feedback on regional air quality – a case study with WRF/Chem, Atmos. Environ., 53, 202–211, 2012.

Fountoukis, C. and Nenes, A.: ISORROPIA II: a computationally efficient thermodynamic equilibrium model for K^+–Ca^{2+}–Mg^{2+}–NH_4^+–Na^+–SO_4^{2-}–NO_3^-–Cl^-–H_2O aerosols, Atmos. Chem. Phys., 7, 4639-4659, 2007.

Fu, C. B., Wang, S. Y., Xiong, Z., Gutowski, W. J., Lee, D., Mcgregor, J. L., Sato, Y., Kato, H., Kim, J., and Suh, M.: Regional climate model intercomparison project for Asia, Bull. Amer. Meteor. Soc., 86, 257-266, 2005.

Fu, H. and Chen, J.: Formation, features and controlling strategies of severe haze-fog pollutions in China, Sci. Total. Environ., 578, 121–138, 2017.

Gao, M., Carmichael, G. R., Wang, Y., Saide, P. E., Yu, M., Xin, J., Liu, Z., and Wang, Z.: Modeling study of the 2010 regional haze event in the North China Plain, Atmos. Chem. Phys., 16, 1673-1691, 10.5194/acp-16-1673-2016, 2016.

Gao, M., Han, Z., Liu, Z., Li, M., Xin, J., Tao, Z., Li, J., Kang, J., Huang, K., Dong, X., Zhuang, B., Li, S., Ge, B., Wu, Q., Cheng, Y., Wang, Y., Lee, H., Kim, C., Fu, J. S., Wang, T., Chin, M., Woo, J., Zhang, Q., Wang, Z., and Carmichael G. R.: Air Quality and Climate Change, Topic 3 of the Model Inter-Comparison Study for Asia Phase III (MICS-Asia III), Part I: overview and model evaluation, Atmos. Chem. Phys., 18, 4859–4884, https://doi.org/10.5194/acp-18-4859-2018, 2018.

Gao, M., Han, Z. W., Tao, Z. N., Li, J. W., Kang, J.-E., Huang, K., Dong, X. Y., Zhuang, B. L., Li, S., Ge, B. Z., Wu, Q. Z., Lee, H.-J., Kim, C. H., Fu, J. S., Wang, T. J., Chin, M., Li, M., Woo, J.-H., Zhang, Q., Cheng, Y. F., Wang, Z. F., and Carmichael, G. R.: Air quality and climate change, Topic 3 of the Model Inter-Comparison Study for Asia Phase III (MICS-Asia III) – Part 2: aerosol radiative effects and aerosol feedbacks. Atmospheric Chemistry and Physics, 20, 1147–1161, 2020.

Gao, Y., Zhang, M., Liu, Z., Wang, L., Wang, P., Xia, X., Tao, M., and Zhu, L.: Modeling the feedback between aerosol and meteorological variables in the atmospheric boundary layer during a severe fog–haze event over the North China Plain, Atmos. Chem. Phys., 15, 4279-4295, 10.5194/acp-15-4279-2015, 2015.

Gery, M.W., Whitten, G.Z., Killus, J.P., and Dodge, M.C.: A photochemical kinetics mechanism for urban and regional scale computer modeling, J. Geophys. Res., 94, 12925-12956, 1989.

Ghan, S. and Zaveri R.A.: Parameterization of optical properties for hydrated internally mixed aerosol, J. Geophys. Res., 112, D10201, doi:10.1029/2006JD007927, 2007.

Giglio, L., Randerson, J. T., and van der Werf, G. R.: Analysis of daily, monthly, and annual burned area using the fourth generation Global Fire Emissions Database (GFED4), J. Geophys. Res.: Biogeosciences, doi:10.1002/jgrg.20042, 2013.

Grell, G. A.: Prognostic evaluation of assumptions used by cumulus parameterizations, Mon. Weather. Rev., 121, 764-787, 1993.

Guo, S., Hu, M., Zamora, M. L., Peng, J., Shang, D., Zheng, J., Du, Z., Wu, Z., Shao, M., Zeng, L., Molina, M. J., and Zhang, R. : Elucidating severe urban haze formation in China, P.

Natl. Acad. Sci. USA., 111, 17373–17378, https://doi.org/10.1073/pnas.1419604111, 2014.
Han, X., Zhang, M. G., Han, Z. W., Xin, J. Y., and Liu, X. H.: Simulation of aerosol direct radiative forcing with RAMS-CMAQ in East Asia, Atmos. Environ., 45, 6576-6592, 2011a.
Han, Z. W., Ueda, H., Matsuda, K., Zhang, R. J., Arao, K., Kanai, Y., and Hasome, H.: Model study on particle size segregation and deposition during Asian dust events in March 2002, J. Geophys. Res., 109, D19205, doi: 10.1029/2004jd004920, 2004.
Han, Z. W.: Direct radiative effect of aerosols over East Asia with a Regional coupled Climate/Chemistry model, Meteorol. Z., Vol. 19, No. 3, 287-298, 2010.
Han, Z. W., Xiong, Z., and Li, J. W.: Direct climatic effect of aerosols and interdecadal variations over East Asia investigated by a regional climate/chemistry model, Atmospheric and Oceanic Science Letters, 4(6), 299-303, 2011b.
Han, Z. W., Li, J. W., Xia, X. A., and Zhang, R. J.: Investigation of direct radiative effects of aerosols in dust storm season over East Asia with an online coupled regional climate-chemistry-aerosol model, Atmos. Environ., 54, 688-699, 2012.
Han, Z. W., Li, J. W., Guo, W. D., Xiong, Z., and Zhang, W.: A study of dust radiative feedback on dust cycle and meteorology over East Asia by a coupled regional climate-chemistry-aerosol model, Atmos. Environ., 68, 54-63, 2013.
Han, Z. W., Li, J. W., Yao, X. H., and Tan, S. C.: A regional model study of the characteristics and indirect effects of marine primary organic aerosol in springtime over East Asia, Atmos. Environ., 197, 22–35, 2019.
Hegg D. A.: Cloud condensation nucleus-sulfate mass relationship and cloud albedo. J. Geophys. Res. Atmos., 99, D12, 25903-25907, 1994.
Hess, M., Koepke, P., and Schuit, I.: Optical properties of aerosols and clouds: the software package OPAC, Bull. Amer. Meteor. Soc., 79, 831-844 ,1998.
Heo, B.-H., Jacoby-Koaly, S., Kim, K.-E., Campistron, B., Benech, B., and Jung, E.-S.: Use of the Doppler Spectral Width to Improve the Estimation of the Convective Boundary Layer Height from UHF Wind Profiler Observations, J. Atmos. Ocean. Technol., 20, 408-424, 2003.
Hong, S. and Pan, H.: Nonlocal boundary layer vertical diffusion in a medium-range forecast model, Mon. Weather Rev., 124, 2322–2339, 1996.
Huang, R. J., Zhang, Y., Bozzetti, C., Ho, K. F., Cao, J. J., Han, Y., Daellenbach, K. R., Slowik, J. G., Platt, S. M., Canonaco, F., Zotter, P., Wolf, R., Pieber, S. M., Bruns, E. A., Crippa, M., Ciarelli, G., Piazzalunga, A., Schwikowski, M., Abbaszade, G., Schnelle-Kreis, J., Zimmermann, R., An, Z., Szidat, S., Baltensperger, U., El Haddad, I., and Prevot, A. S.: High secondary aerosol contribution to particulate pollution during haze events in China, Nature, 514, 218-222, 10.1038/nature13774, 2014.
Huang, X., Wang, Z. L., Ding, A. J.: Impact of Aerosol-PBL Interaction on Haze Pollution: Multiyear Observational Evidences in North China, Geophys. Res. Lett., 45, 8596-8603, 2018.
Isaksen I.S.A., Granier, C., Myhre, G., Berntsen, T.K., Dalsøren, S.B., Gauss, M., Klimont, Z., Benestad, R., Bousquet, P., Collins, W., Cox, T., Eyring, V., Fowler, D., Fuzzi, S., Jo¨ckel, P., Laj, P., Lohmann, U., Maione, M., Monks, P., Prevot, A.S.H., Raes, F., Richter,

A., Rognerud, B., Schulz, M., Shindell, D., Stevenson, D.S., Storelvmo, T., Wang, W.-C., van Weele, M., Wild, M., and Wuebbles, D.: Atmospheric composition change: Climate–Chemistry interactions, Atmos. Environ., 43, 5138–5192, 2009.

Jing, J., Wu, Y., Tao, J., Che, H.Z, Xia, X., Zhang, X., Yan, P., Zhao, D.M., and Zhang, L.M.: Observation and analysis of near-surface atmospheric aerosol optical properties in urban Beijing, Particuology, 18, 144-154, 2015.

Kajino, M., Ueda, H., Han, Z. W., Kudo, R., Inomata, Y., Kaku, H.: Synergy between air pollution and urban meteorological changes through aerosol-radiation-diffusion feedback—A case study of Beijing in January 2013, Atmos. Environ., 171, 98-110, 2017.

Keihl, J.T., Hack, J.J., Bonan, G.B., Boville, B.A., Briegleb, B.P., Williamson, D.L., and Rasch, P.J.: Description of the NCAR Community Climate Model (CCM3), NCAR Technical Note, NCAR/TN-420+STR, p.152 , 1996.

Lee-Taylor, J., Madronich, S.: Climatology of UV-A, UV-B, and Erythemal Radiation at the Earth's Surface, 1979-2000, NCAR Technical Note, NCAR/TN-474+STR, pp 1-52. 2007.

Li, G.H., Bei, N.F., Cao, J.J., Huang, R.J., Wu, J.R., Feng, T., Wang, Y.C., Liu, S.X., Zhang, Q., Tie, X.X., and Molina, L.T.: A possible pathway for rapid growth of sulfate during haze days in China, Atmos. Chem. Phys., 17, 3301-3316, 2017c.

Li, J., Chen, X.S., Wang, Z.F., Du, H.Y., Yang, W.Y., Sun, Y.L., Hu, B., Li, J.J., Wang, W., Wang, T., Fu, P.Q., and Huang, H.L.: Radiative and heterogeneous chemical effects of aerosols on ozone and inorganic aerosols over East Asia, Sci. Total. Environ., 622–623, 1327–1342 , 2018b.

Li, J. W. and Han, Z. W.: A modeling study of the impact of heterogeneous reactions on mineral aerosol surfaces on tropospheric chemistry over East Asia, Particuology, 8, 433-441, 2010.

Li, J. W., Han, Z. W., and Zhang, R. J.: Influence of aerosol hygroscopic growth parameterization on aerosol optical depth and direct radiative forcing over East Asia, Atmos. Res., 140-141, 14-27, 2014.

Li, J. W. and Han, Z. W.: A modeling study of severe winter haze events in Beijing and its neighboring regions, Atmos. Res., 170, 87–97, 2016a.

Li, J. W. and Han, Z. W.: Aerosol vertical distribution over east China from RIEMS-Chem simulation in comparison with CALIPSO measurements, Atmos. Environ., 143, 177-189, 2016b.

Li, J. W. and Han, Z. W.: Seasonal variation of nitrate concentration and its direct radiative forcing over East Asia, Atmosphere, 7(8), 105, 2016c.

Li, J. W., Han, Z. W., and Yao, X. H.: A modeling study of the influence of sea salt on inorganic aerosol concentration, size distribution, and deposition in the western Pacific Ocean, Atmos. Environ., 188, 157-173, 2018a.

Li, J. W., Han, Z. W., Yao, X. H., Xie, Z. X., and Tan, S. C.: The distributions and direct radiative effects of marine aerosols over East Asia in springtime, Sci. Total. Environ., 651, 1913–1925, 2019b.

Li, M., Zhang, Q., Kurokawa, J.-I., Woo, J.-H., He, K., Lu, Z., Ohara, T., Song, Y., Streets, D. G., Carmichael, G. R., Cheng, Y., Hong, C., Huo, H., Jiang, X., Kang, S., Liu, F., Su, H., and Zheng, B.: MIX: a mosaic Asian anthropogenic emission inventory under the international collaboration framework of the MICS-Asia and HTAP, Atmos. Chem. Phys., 17, 935-963, 10.5194/acp-17-935-2017, 2017a.

Li, X., Wu, J., Elser, M., Tong, S., Liu, S., Li, X., Liu, L., Cao, J., Zhou, J., El-Haddad, I., Huang, R., Ge, M., Tie, X., André S. H. Prévôt, and Li, G.: Wintertime secondary organic aerosol formation in Beijing–Tianjin–Hebei (BTH): contributions of HONO sources and heterogeneous reactions, Atmos. Chem. Phys., 19, 2343–2359, https://doi.org/10.5194/acp-19-2343-2019, 2019a.

Li, Z., Guo, J., Ding, A., Liao, H., Liu, J., Sun, Y., Wang, T., Xue, H., Zhang, H., and Zhu, B.: Aerosol and boundary-layer interactions and impact on air quality, Natl. Sci. Rev., 4, 810–833, 10.1093/nsr/nwx117, 2017b.

Liu, X. H. and Wang, J.: How important is organic aerosol hygroscopicity to aerosol indirect forcing? Environ. Res. Lett., 5(4), 044010, http://iopscience.iop.org/1748-9326/5/4/044010, 2010a.

Liu, X. H., Zhang, Y., Xing, J., Zhang, Q., Wang, K., Streets, D., Jang, C., Wang, W.-X., and Hao, J.-M.: Understanding of regional air pollution over China using CMAQ, part II. Process analysis and sensitivity of ozone and particulate matter to precursor emissions, Atmos. Environ., 44, 3719-3727, 2010b.

Ma, N., Zhao, C. S., Müller, T., Cheng, Y. F., Liu, P. F., Deng, Z. Z., Xu, W. Y., Ran, L., Nekat, B., van Pinxteren, D., Gnauk, T., Müller, K., Herrmann, H., Yan, P., Zhou, X.J., and Wiedensohler, A.: A new method to determine the mixing state of light absorbing carbonaceous using the measured aerosol optical properties and number size distributions, Atmos. Chem. Phys., 12, 2381–2397, 2012.

Ma, Q. X., Wu, Y. F., Zhang, D. Z., Wang, X. J., Xia, Y. J., Liu, X. Y., Tian, P., Han, Z. W., Xia, X. A., Wang, Y., and Zhang, R. J.: Roles of regional transport and heterogeneous reactions in the $PM_{2.5}$ increase during winter haze episodes in Beijing, Sci. Total. Environ., 599–600, 246–253, 2017.

Martin, G. M., Johnson, D. W., and Spice, A.: The Measurements and Parameterization of Effective Radius of Droplets in Warm Stratocumulus Clouds, J. Atmos. Sci., 51, 1823–1842, 1994.

NOAA/NCEP.: NCEP FNL Operational Model Global Tropospheric Analyses, continuing from July 1999. Research Data Archive at the National Center for Atmospheric Research, Computational and Information Systems Laboratory, Dataset. https://doi.org/10.5065/D6M043C6, Last accessed, 12 April 2019, 2000.

Odum, J.R., Jungkamp, T.P.W., Griffin, R.J., Flagan, R.C., and Seinfeld, J.H.: The atmospheric aerosol-forming potential of whole gasoline vapor, Science. 276, 96–99, 1997.

Petters, M.D. and Kreidenweis, S.M.: A single parameter representation of hygroscopic growth and cloud condensation nucleus activity, Atmos. Chem. Phys., 7, 1961-1971, 2007.

Qiu, Y., Liao, H., Zhang, R., and Hu, J.: Simulated impacts of direct radiative effects of scattering and absorbing aerosols on surface layer aerosol concentrations in China during a heavily polluted event in February 2014, J. Geophys. Res. Atmos., 122, 5955-5975, 10.1002/2016jd026309, 2017.

Ramanathan, V., Crutzen, P. J., Kiehl, J. T., and Rosenfeld, D.: Aerosols, climate, and the hydrological cycle, Science, 294, 2119-2124, 10.1126/science.1064034, 2001.

Riemer, N., West, M., Zaveri, R., and Easter, R.: Estimating black carbon aging time-scales with a particle-resolved aerosol model, J. Aerosol Sci., 41, 143-158, 2010.

Song, Z.J., Fu, D.S., Zhang, X.L., Wu, Y.F., Xia, X.A., He, J.X., Han, X.L., Zhang, R.J., and

Che, H.Z.: Diurnal and seasonal variability of $PM_{2.5}$ and AOD in North China plain: Comparison of MERRA-2 products and ground measurements, Atmos. Environ., 191, 70-78, 2018.

Sun, Y., Jiang, Q., Wang, Z., Fu, P., Li, J., Yang, T., and Yin, Y.: Investigation of the Sources and Evolution Processes of Severe Haze Pollution in Beijing in January 2013, J. Geophys. Res., 119, 4380–4398, 2014.

Tao, Z. N., Chin, M., Gao, M., Kucsera, T., Kim, D.-C., Bian, H. S., Kurokawa, J.-I., Wang, Y. S., Liu, Z. R., Carmichael, G. R., Wang, Z. F., and Akimoto, H.: Evaluation of NU-WRF model performance on air quality simulation under various model resolutions – an investigation within the framework of MICS-Asia Phase III. Atmos. Chem. Phys., 20, 2319–2339, 2020.

Twomey, S.: Pollution and the planetary albedo, Atmos. Environ., 8, 1251–1256, 1974.

Wang, J., Wang, S., Jiang, J., Ding, A., Zheng, M., Zhao, B., Wong, D. C., Zhou, W., Zheng, G., and Wang, L.: Impact of aerosol-meteorology interactions on fine particle pollution during China's severe haze episode in January 2013, Environ. Res. Lett., 9, 094002, https://doi.org/10.1088/1748-9326/9/9/094002, 2014b.

Wang, S. Y., Fu, C. B., Wei, H. L., Qian, Y., Xiong, Z., Feng, J.M., Zhao, D. M., Dan, L., Han, Z.W., Su, B.K., Zhao, M., Zhang, Y.C., Tang, J.P., Liu, H.N., Wu, J., Zeng, X.M., Chen, M., and Wang, L.Z.: Regional integrated environmental modeling system: development and application, Climate Change, 129, 499-510, 2015.

Wang, Y., Bao, S., Wang, S., Hu, Y., Shi, X., Wang, J., Zhao, B., Jiang, J., Zheng, M., Wu, M., Russell, A. G., Wang, Y., and Hao, J.: Local and regional contributions to fine particulate matter in Beijing during heavy haze episodes, Sci. Total. Environ., 580, 283-296, 10.1016/j.scitotenv.2016.12.127, 2017.

Wang, Z. L., Huang, X., Ding, A. J.: Dome effect of black carbon and its key influencing factors: a one-dimensional modelling study, Atmos. Chem. Phys., 18, 2821–2834, 2018.

Wang, Z., Li, J., Wang, Z., Yang, W., Tang, X., Ge, B., Yan, P., Zhu, L., Chen, X., Chen, H., Wand, W., Li, J., Liu, B., Wang, X., Wand, W., Zhao, Y., Lu, N., and Su, D.: Modeling study of regional severe hazes over mid-eastern China in January 2013 and its implications on pollution prevention and control, Sci. China. Earth. Sci., 57, 3-13, 10.1007/s11430-013-4793-0, 2014a.

Westervelt, D. M., Moore, R. H., Nenes, A. and Adams, P.J.: Effect of primary organic sea spray emissions on cloud condensation nuclei concentrations, Atmos. Chem. Phys., 12, 89–101, 2012.

Wilcox, E. M., Thomas, R. M., Praveen, P. S., Pistone, K., Bender, F. A., and Ramanathan, V.: Black carbon solar absorption suppresses turbulence in the atmospheric boundary layer. Proc. Natl. Acad. Sci. USA, 113(42), 11794–11799, 2016.

Wu, J., Bei, N., Hu, B., Liu, S., Zhou, M., Wang, Q., Li, X., Liu, L., Feng, T., Liu, Z., Wang, Y., Cao, J., Tie, X., Wang J., Molina, L.T., and Li, G.: Aerosol–radiation feedback deteriorates the wintertime haze in the North China Plain, Atmos. Chem. Phys., 19, 8703–8719, https://doi.org/10.5194/acp-19-8703-2019, 2019.

Wu, Y. F., Zhang, R. J., Tian, P., Tao, J., Hsu, S.-C., Yan, P., Wang, Q. Y., Cao, J. J., Zhang, X. L., and Xia, X. A.: Effect of ambient humidity on the light absorption amplification of black carbon in Beijing during January 2013, Atmos. Environ., 124, 217-223 , 2016.

Xiong, Z., Fu, C. B., and Yan, X. D.: Regional Integrated environmental model system and its simulation of East Asia summer monsoon, Chinese. Sci. Bull., 54(22), 4253-4261, 2009.

Yu, S., Mathur, R., Schere, K., Kang, D., Plein, J., Young, J., Tong, D., Pouliot, G., Mckeen, S.A., and Rao, S. T.: Evaluation of real-time $PM_{2.5}$ forecasts and process analysis for $PM_{2.5}$ formation over the eastern United States using the Eta-CMAQ forecast model during the 2004 ICARTT study, J. Geophys. Res., 113, D06204, doi: 10.1029/2007JD009226, 2008.

Zhang, B., Wang, Y., and Hao, J.: Simulating aerosol–radiation–cloud feedbacks on meteorology and air quality over eastern China under severe haze conditions in winter, Atmos. Chem. Phys., 15, 2387-2404, 10.5194/acp-15-2387-2015, 2015.

Zhang, X. Y., Wang, Y. Q., Niu, T., Zhang, X. C., Gong, S. L., Zhang, Y. M., and Sun, J. Y.: Atmospheric aerosol compositions in China: spatial/temporal variability, chemical signature, regional haze distribution and comparisons with global aerosols, Atmos. Chem. Phys., 12, 779–799, https://doi.org/10.5194/acp-12-779-2012, 2012.

Zhang, X., Zhong, J., Wang, J., Wang, Y., and Liu, Y.: The interdecadal worsening of weather conditions affecting aerosol pollution in the Beijing area in relation to climate warming, Atmos. Chem. Phys., 18, 5991–5999, https://doi.org/10.5194/acp-18-5991-2018, 2018a.

Zhang, X., Zhang, Q., Hong, C., Zheng, Y., Geng, G., Tong, D., Zhang, Y. and Zhang, X.: Enhancement of $PM_{2.5}$ Concentrations by Aerosol-Meteorology Interactions Over China, J. Geophys. Res. Atmos., 123, https://doi.org/10.1002/2017JD027524, 2018b.

Zhang, Y.: Online coupled meteorology and chemistry models: history, current status, and outlook, Atmos. Chem. Phys., 8, 2895-2932,2008.

Zhang, Y., Wen, X.-Y., Wang, K., Vijayaraghavan, K., and Jacobson, M. Z.: Probing into regional O_3 and PM pollution in the U.S., PartII. An examination of formation mechanisms through a process analysis technique and sensitivity study, J. Geophys. Res.,114 (D22305), doi:10.1029/2009JD011900, 2009.

Zhang, Y., Wen, X. Y., and Jang, C. J.: Simulating chemistry-aerosol-cloud-radiation-climate feedbacks over the continental U.S. using the online-coupled weather research forecasting model with chemistry (WRF/Chem), Atmos. Environ., 44, 3568–3582, 2010.

Zhao, B., Liou, K. N., Gu, Y., Li, Q., Jiang, J. H., Su, H., He, C., Tseng, H. R., Wang, S., Liu, R., Qi, L., Lee, W. L., and Hao, J.: Enhanced $PM_{2.5}$ pollution in China due to aerosol-cloud interactions, Sci. Rep., 7, 4453, 10.1038/s41598-017-04096-8, 2017.

Zhao, D. M.: Performance of Regional Integrated Environment Modeling System (RIEMS) in precipitation simulations over East Asia, Clim. Dynam. 40, 1767-1787, 2013.

Zhao, P., Dong, F., Yang, Y., He, D., Zhao, X., and Zhang, W.: Characteristics of carbonaceous aerosol in the region of Beijing, Tianjin, and Hebei, China, Atmos. Environ., 71, 389–398, 2013.

Zheng, B., Zhang, Q., Zhang, Y., He, K. B.,Wang, K., Zheng, G. J., Duan, F. K., Ma, Y. L., and Kimoto, T.: Heterogeneous chemistry: a mechanism missing in current models to explain secondary inorganic aerosol formation during the January 2013 haze episode in North China, Atmos. Chem. Phys., 15, 2031–2049, doi:10.5194/acp-15-2031-2015, 2015.

Zhong, J., Zhang, X., Dong, Y.,Wang, Y., Liu, C.,Wang, J., Zhang, Y., and Che, H.: Feedback effects of boundary-layer meteorological factors on cumulative explosive growth of $PM_{2.5}$ during winter heavy pollution episodes in Beijing from 2013 to 2016, Atmos. Chem. Phys., 18, 247–258, https://doi.org/10.5194/acp-18-247-2018, 2018a.

Zhong, J., Zhang, X., Wang, Y., Liu, C., and Dong, Y.: Heavy aerosol pollution episodes in winter Beijing enhanced by radiative cooling effects of aerosols, Atmos. Res., 209, 59–64, https://doi.org/10.1016/j.atmosres.2018.03.011, 2018b.

Zhuang, B. L., Li, S., Wang, T. J., Deng, J. J., Xie, M., Yin, C. Q., and Zhu, J. L.: Direct radiative forcing and climate effects of anthropogenic aerosols with different mixing states over China, Atmos. Environ., 79, 349-361, 2013.

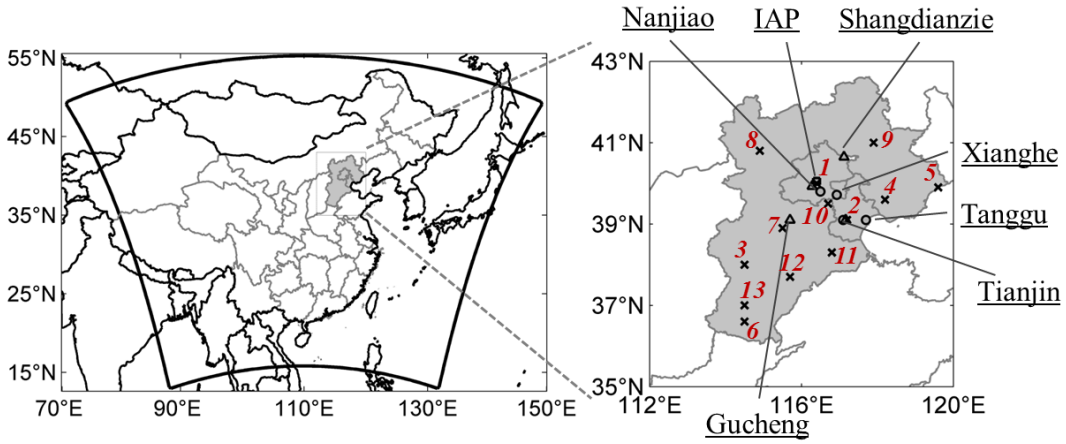

Figure 1. The model study domain. The shaded areas indicate the Beijing-Tianjin-Hebei (BTH) region. Markers are observation sites (square: IAP, observations of $PM_{2.5}$, its chemical components, aerosol extinction coefficient (EXT) and aerosol absorption coefficient (ABS); circles: observations of meteorological variables; triangles: aerosol optical depth (AOD). The Xianghe site provides meteorological soundings and hourly surface shortwave radiation (SWDOWN) measurements; the Tianjin site provides both meteorological variables and AOD). Hourly O_3, SO_2, NO_2 and $PM_{2.5}$ measurements at 13 cities from the CNEMC (China National Environmental Monitoring Center, http://www.cnemc.cn/) are labeled by crosses with numbers (1-Beijing, 2-Tianjin, 3-Shijiazhuang, 4-Tangshan, 5-Qinhuangdao, 6-Handan, 7-Baoding, 8-Zhangjiakou, 9-Chengde, 10-Langfang, 11-Cangzhou, 12-Hengshui and 13-Xingtai).

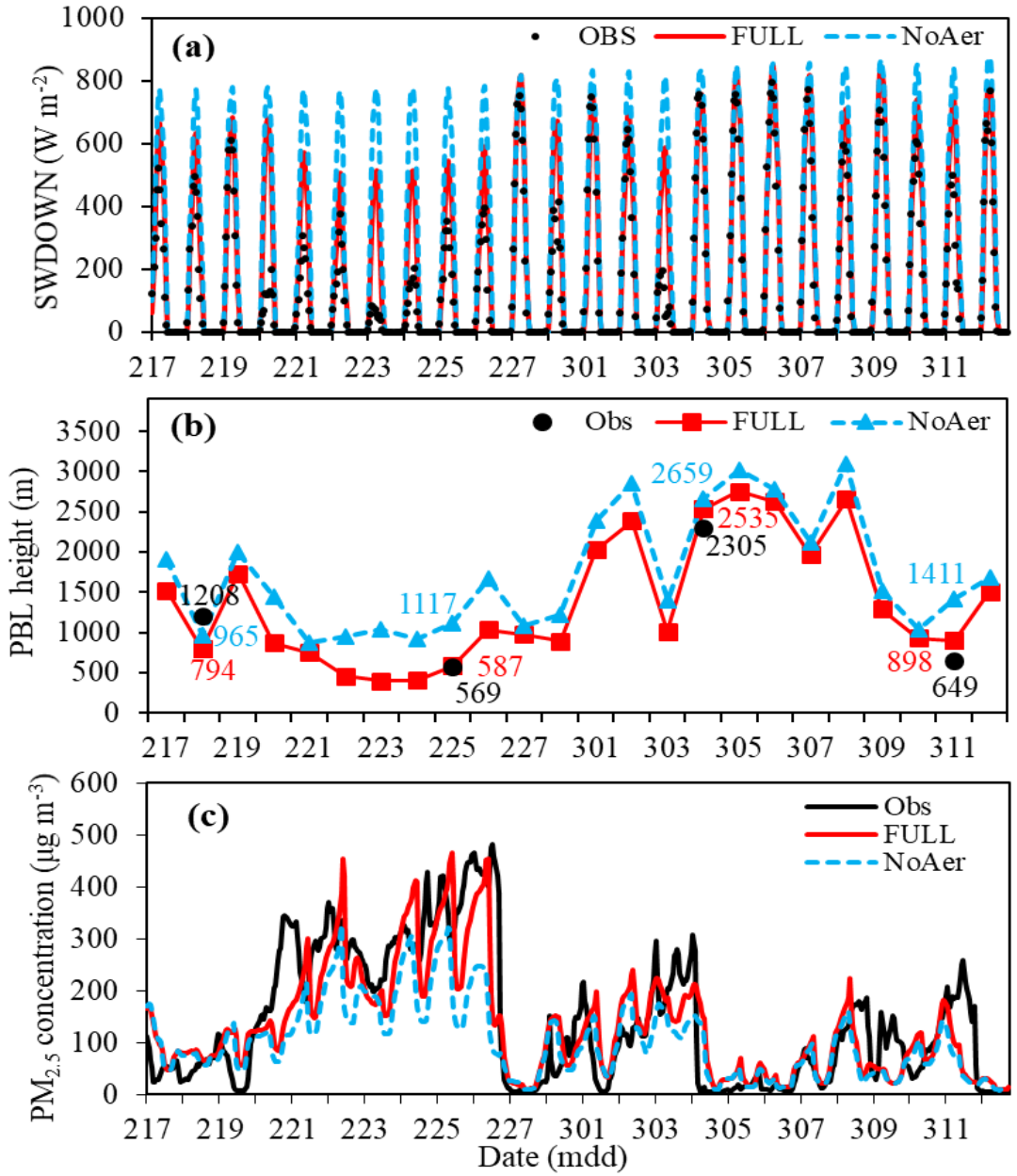

Figure 2. The model simulated and observed (a) hourly SWDOWN at Xianghe, (b) hourly PBL height at 14:00 (LST) at Xianghe (note observations are available in the 4 days, numbers are observations and corresponding simulations) and (c) hourly $PM_{2.5}$ concentration at IAP in Beijing.

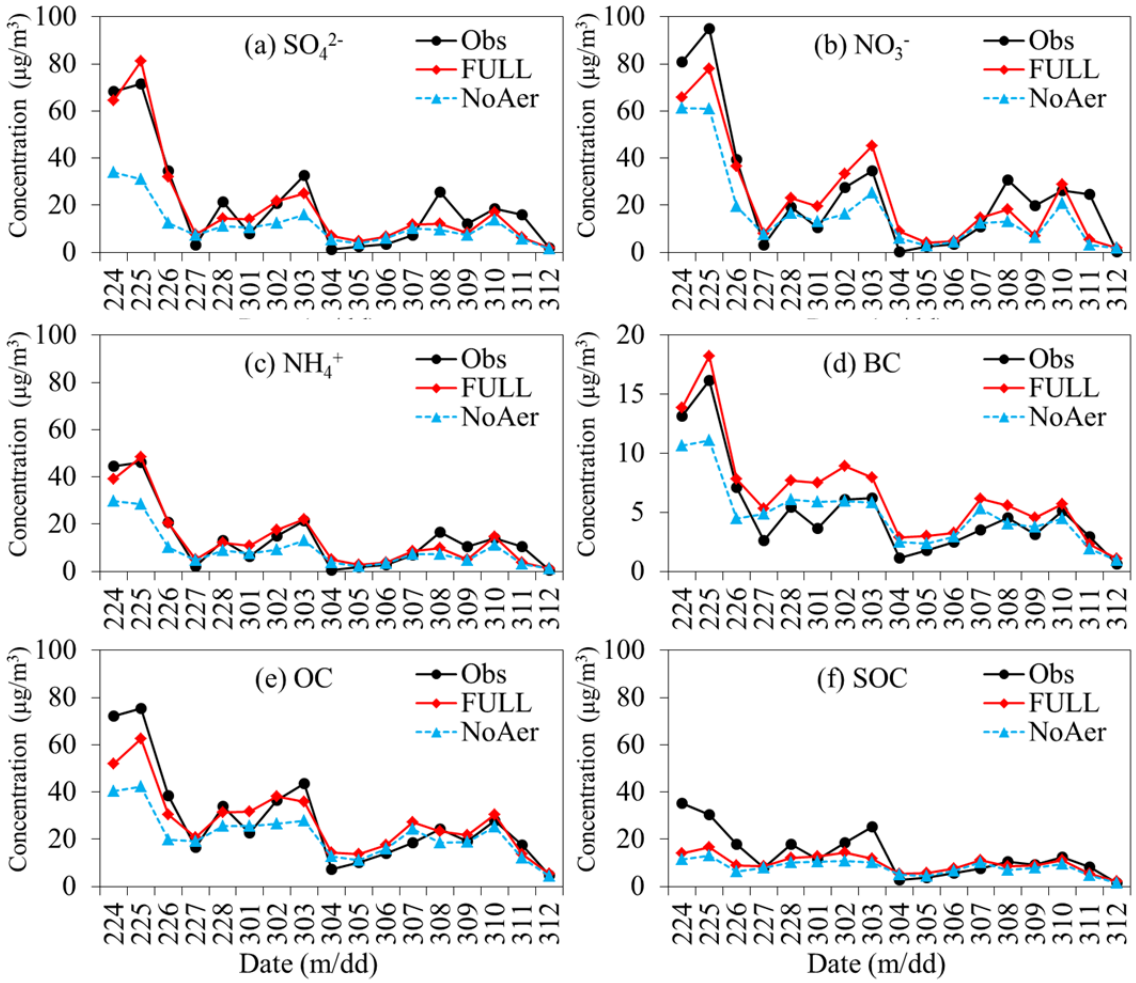

1677

1678 Figure 3. The model simulated and observed daily mean concentrations of aerosol

1679 compositions in $PM_{2.5}$ at the IAP site in Beijing.

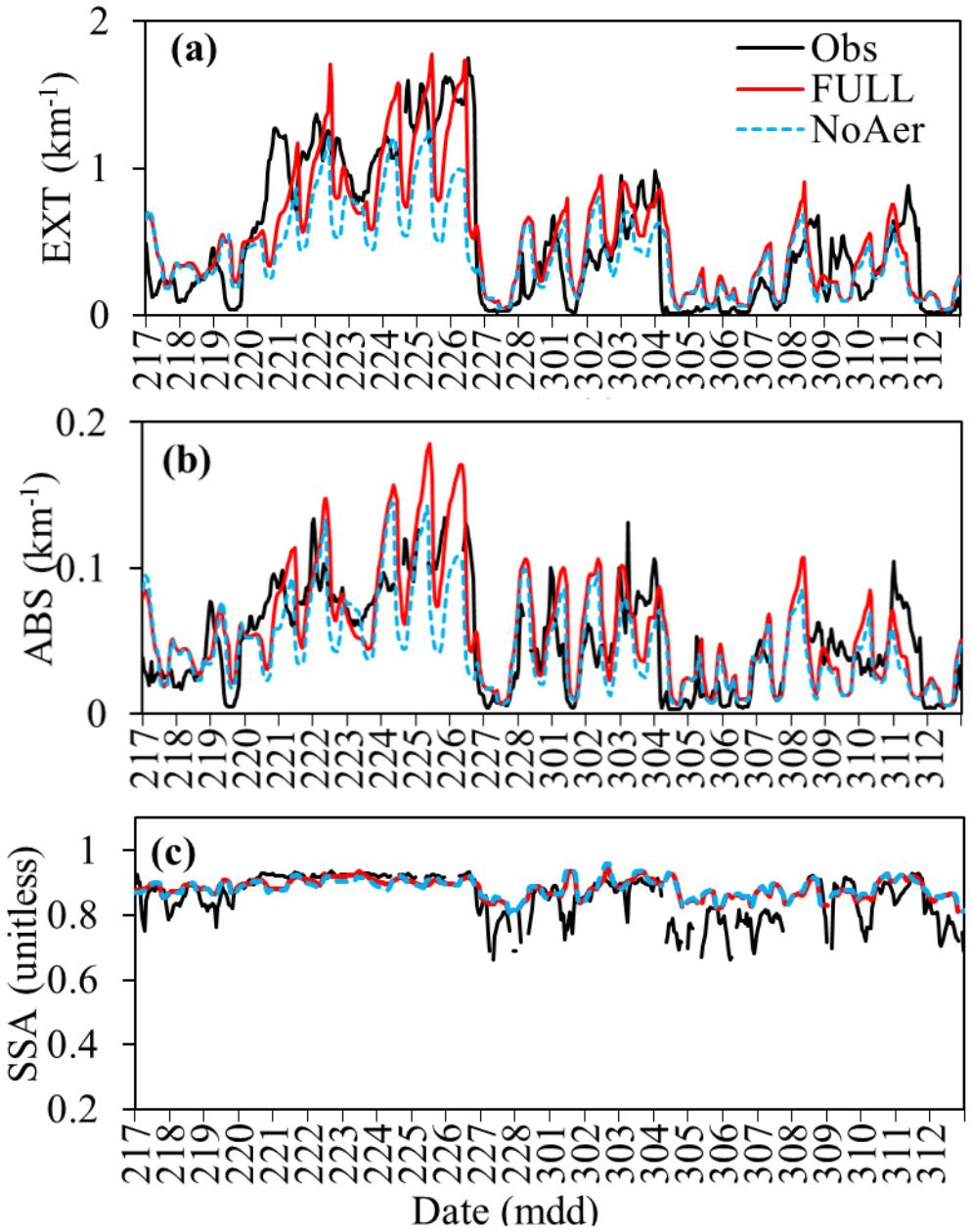

Figure 4. The model simulated and observed hourly (a) aerosol extinction coefficient (EXT), (b) absorption coefficient (ABS) and (c) single scattering albedo (SSA) at the IAP site in Beijing under dry condition (RH=10%).

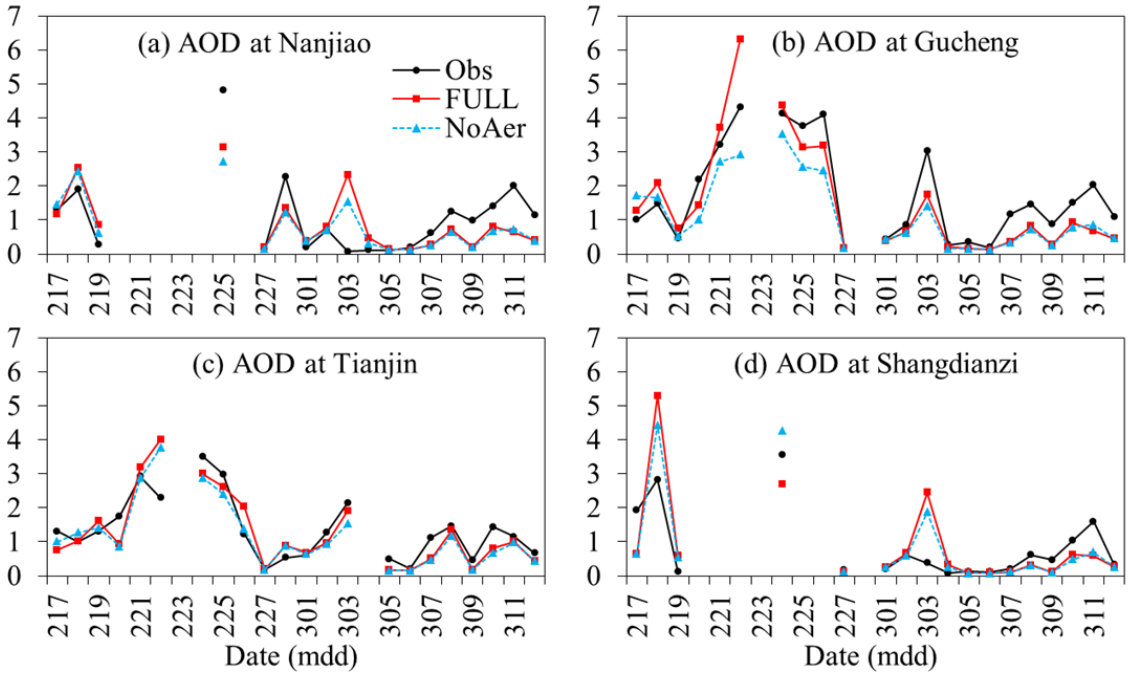

Figure 5. The model simulated and observed daily mean AOD (at 550 nm) at the four sites of CARSNET.

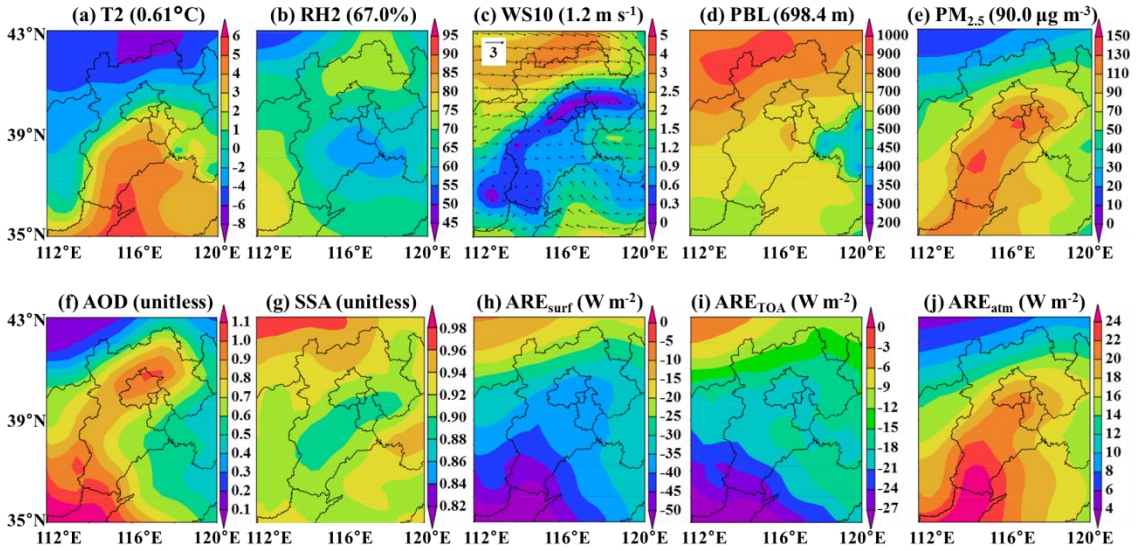

Figure 6. The model simulated (a) air temperature (T2), (b) relative humidity (RH2), (c) wind speed (WS10), (d) PBL height, (e) $PM_{2.5}$ concentration, (f) AOD, (g) SSA, (h) all-sky ARE at the surface, (i) all-sky ARE at the top of atmosphere and (j) all-sky ARE in the atmosphere from the FULL case. Numbers in the parentheses are averages over the BTH region during the entire study period.

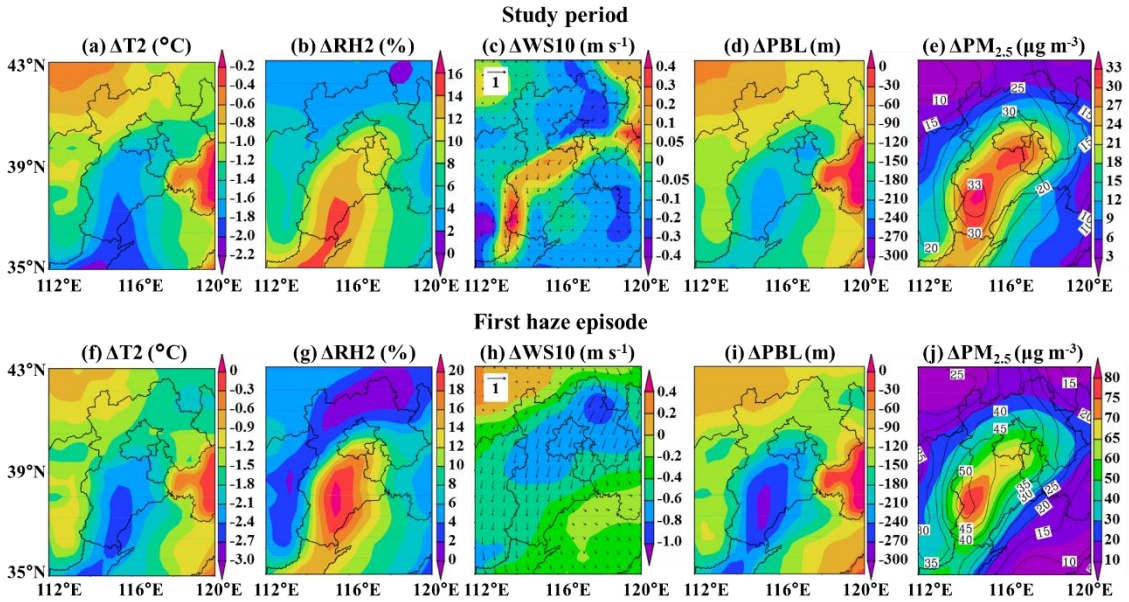

Figure 7. The model simulated feedback-induced changes (FULL minus NoAFB) in (a, f) air temperature (T2), (b, g) relative humidity (RH2), (c, h) wind speed (WS10), (d, i) PBL height and (e, j) $PM_{2.5}$ concentration averaged over the entire study period (a-e) and over the first haze episode (20–26 February) (f-j). Units are given in the parentheses.

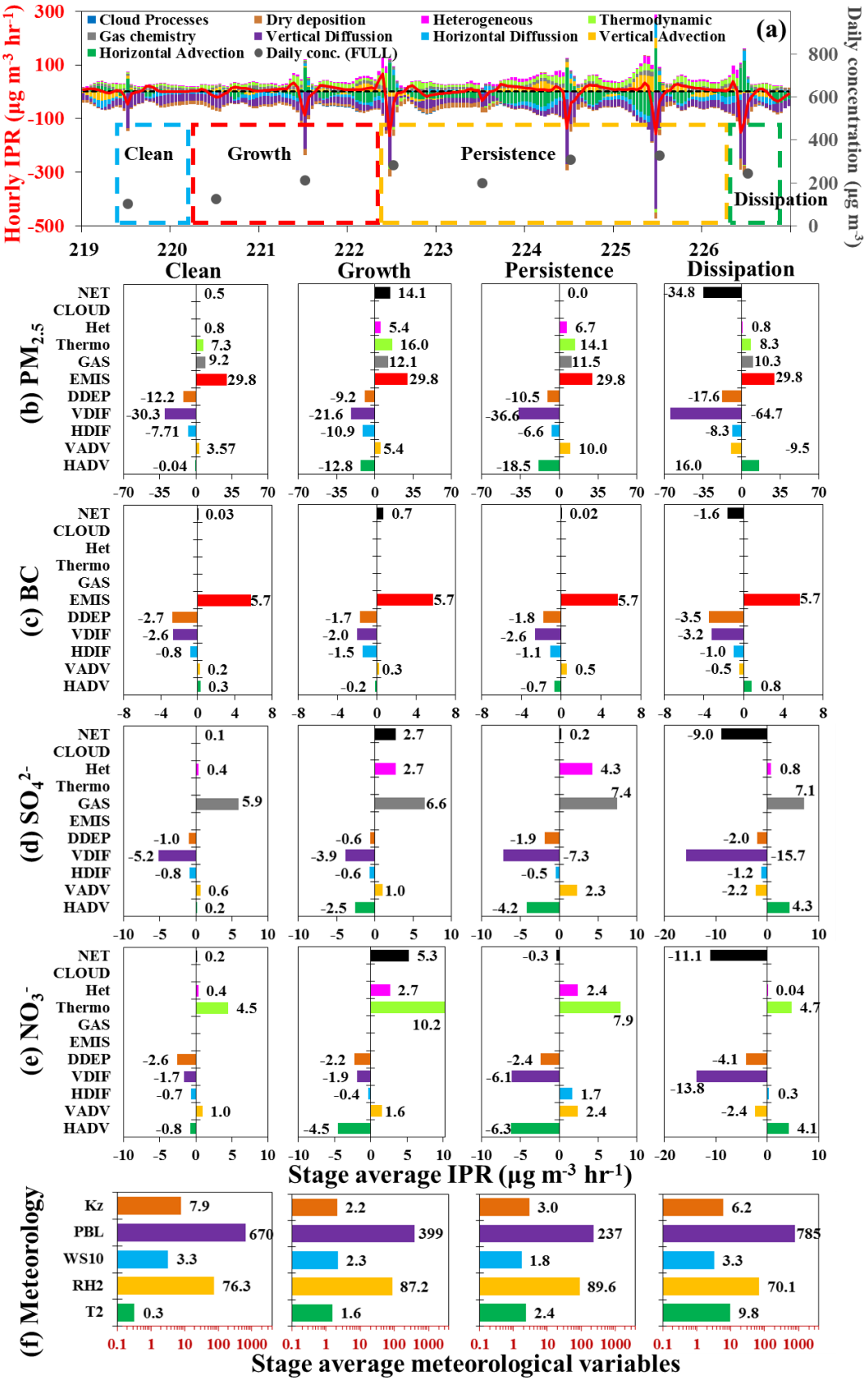

Figure 8. The model calculated integrated process rates (IPR) for the first haze episode (20–26 February) in Beijing. (a) hourly IPR, daily $PM_{2.5}$ concentration and the division of the four stages. The nearly constant IPRs of emissions are not shown for clarity. The mean IPRs for (b) $PM_{2.5}$, (c) BC, (d) sulfate (SO_4^{2-}), (e) nitrate (NO_3^-), and (f) mean meteorological variables in the four stages. Note that zero IPR values are not listed. Units of T2, RH2, WS10, PBL and K_z are °C, %, m s^{-1}, m and m^2 s^{-1}, respectively.

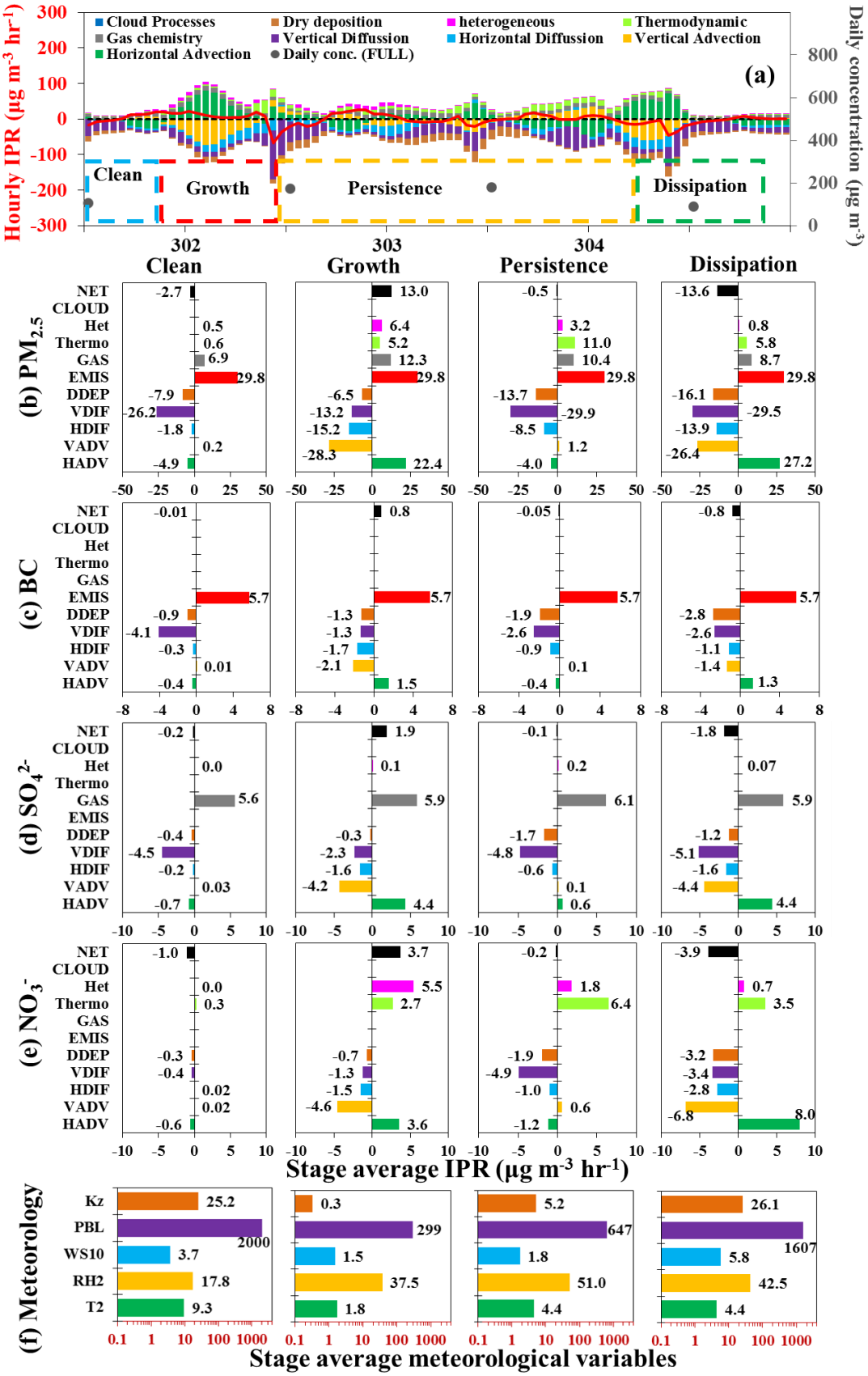

Figure 9. Same as Figure 8 but for the second haze episode (1–4 March).

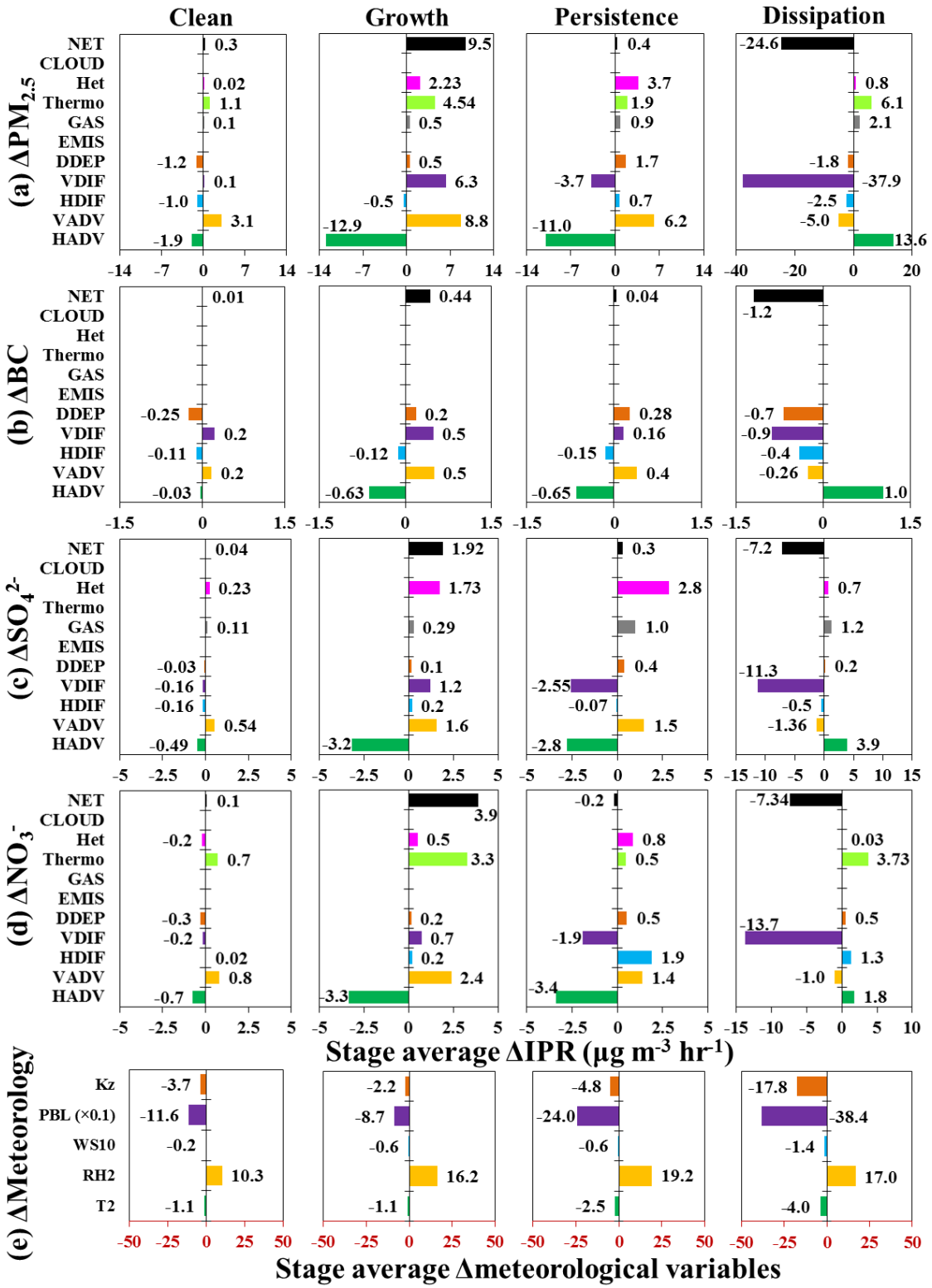

Figure 10. The feedback-induced mean changes in IPRs (FULL minus NoAFB) for $PM_{2.5}$ and its chemical components and meteorological variables during the first haze episode (20–26 February) in Beijing. ΔIPRs for $PM_{2.5}$ and its chemical components and Δmeteorological variables are averages over the four stages. Note that zero ΔIPR values (no change) are not shown and the ΔPBL heights are scaled by 0.1. The division of the four stages and units are the same as those in Figure 8.

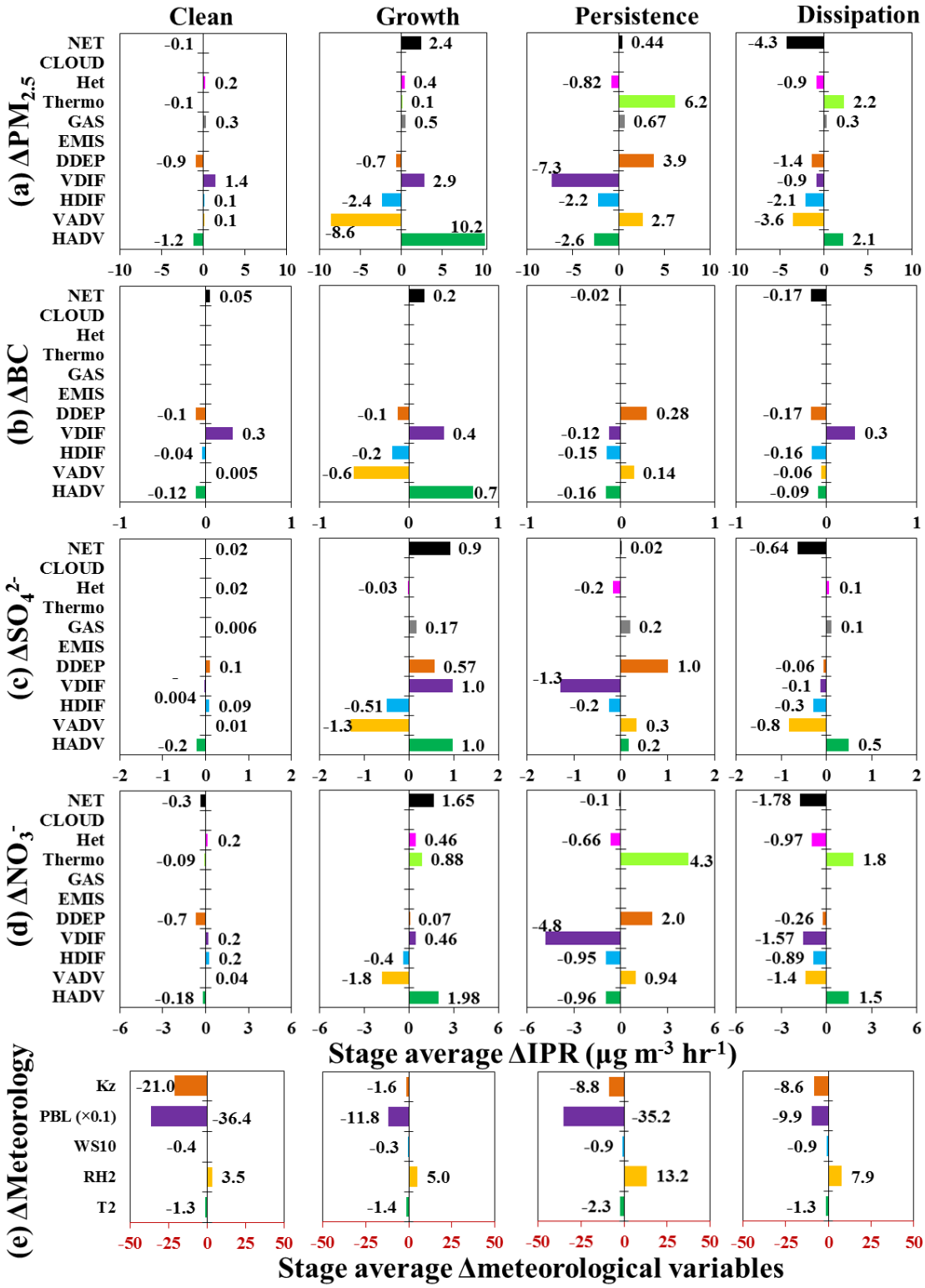

Figure 11. Same as Figure 10 but for the second haze episode (1–4 March). The division of the four stages are the same as that in Figure 9.

Table 1. Performance statistics for meteorological variables at observation sites in the BTH region. Mean observation (Obs), mean simulation (Sim), correlation coefficient (R) and normalized mean bias (NMB in %) are given. WS10, T2 and RH2 are wind speed at 10 meter, air temperature at 2 meter and relative humidity at 2 meter, respectively. All the sample numbers are 207.

Sites	Longitude	Latitude	WS10 ($m\ s^{-1}$)				T2 (°C)				RH2 (%)				SWDOWN ($W\ m^{-2}$)			
			Obs	Sim	R	NMB	Obs	Sim	R	NMB	Obs	Sim	R	NMB	Obs	Sim	R	NMB
FULL																		
Beijing	39°48'N	116°30'E	2.3	2.9	0.53	28%	3.0	2.5	0.77	-16%	53.4	62.6	0.72	17%				
Tianjin	39°6'N	117°6'E	2.6	3.1	0.53	23%	3.5	3.8	0.89	8%	62.9	59.2	0.68	-6%				
Tanggu	39°6'N	117°42'E	2.4	3.4	0.36	42%	3.0	3.1	0.84	2%	69.3	61.3	0.49	-12%				
Total			2.4	3.1	0.47	31%	3.2	3.1	0.83	-2%	61.9	61.0	0.61	-1%				
Xianghe	39°45'N	116°58'E													136.0	188.4	0.91	38%
NoAFB																		
Beijing	39°48'N	116°30'E	2.3	3.4	0.48	48%	3.0	4.1	0.74	37%	53.4	51.1	0.68	-4%				
Tianjin	39°6'N	117°6'E	2.6	3.6	0.48	39%	3.5	5.3	0.88	51%	62.9	47.8	0.65	-24%				
Tanggu	39°6'N	117°42'E	2.4	3.8	0.28	60%	3.0	4.5	0.84	50%	69.3	51.4	0.48	-26%				
Total			2.4	3.6	0.41	49%	3.2	4.6	0.82	46%	61.9	50.1	0.59	-19%				
Xianghe	39°45'N	116°58'E													136.0	234.0	0.85	72%

Table 2. Performance statistics for $PM_{2.5}$ concentration and its chemical components, aerosol optical parameters at RH=10% (EXT, ABS and SSA) at the IAP site in Beijing. Mean observation (Obs), mean simulation (Sim), correlation coefficient (R) and normalized mean bias (NMB in %) are listed.

			FULL			NoAFB		
Species (unit)	Samples	Obs	Sim	R	NMB	Sim	R	NMB
$PM_{2.5}$ ($\mu g\ m^{-3}$)	570	142.0	131.4	0.80	-7%	101.2	0.73	-29%
SO_4^{2-} ($\mu g\ m^{-3}$)	33	21.0	20.3	0.92	-4%	11.9	0.88	-44%
NO_3^- ($\mu g\ m^{-3}$)	33	26.0	24.3	0.88	-6%	17.6	0.87	-32%
NH_4^+ ($\mu g\ m^{-3}$)	33	14.1	13.9	0.91	-2%	9.4	0.89	-34%
BC ($\mu g\ m^{-3}$)	33	5.2	6.7	0.92	28%	5.0	0.84	-3%
OC ($\mu g\ m^{-3}$)	33	29.1	28.3	0.88	-3%	22.3	0.78	-24%
POC ($\mu g\ m^{-3}$)	33	15.5	18.4	0.93	19%	14.1	0.87	-9%
SOC ($\mu g\ m^{-3}$)	33	13.6	9.9	0.56	-27%	8.2	0.45	-40%
EXT (km^{-1})	570	0.51	0.53	0.79	4%	0.41	0.72	-19%
ABS (km^{-1})	534	0.048	0.052	0.68	10%	0.043	0.59	-11%
SSA (unitless)	534	0.85	0.88	0.65	5%	0.88	0.59	5%

Table 3. Performance statistics for daily mean AOD at the four CARSNET sites in the BTH region. Mean observation (Obs), mean simulation (Sim), correlation coefficient (R) and normalized mean bias (NMB, in the unit of %) are listed.

			FULL			NoAFB		
	Samples	Obs	Sim	R	NMB	Sim	R	NMB
Nanjiao	18	1.09	0.92	0.67	-15.6%	0.82	0.74	-24.9%
Gucheng	22	1.73	1.51	0.90	-12.8%	1.16	0.91	-33.0%
Tianjin	22	1.37	1.29	0.86	-5.7%	1.19	0.86	-12.8%
Shangdianzi	17	0.84	0.90	0.72	6.2%	0.89	0.85	5.0%
Total	79	1.29	1.18	0.81	-8.6%	1.03	0.82	-20.2%

Table 4. The model simulated domain and period averages of AOD, SSA and AREs from the FULL case over the BTH region.

	AOD (unitless)	SSA (unitless)	ARE_{surf} (W m^{-2})	ARE_{TOA} (W m^{-2})	ARE_{atm} (W m^{-2})
	Study period (17 February to 12 March)				
All day	0.78	0.91	-37	-18	19
Daytime	1.53	0.92	-79	-39	40
	First haze episode (20–26 February)				
All day	1.59	0.93	-57	-32	25
Daytime	3.17	0.93	-123	-69	53

Table 5. The model simulated feedback-induced changes (FULL minus NoAFB) in T2, WS10, RH2, PBL height, $PM_{2.5}$ concentration and vertical diffusion coefficient (K_z) averaged over the BTH region during the entire period and the first haze episode. Inside the parentheses are percentage changes relative to the NoAFB case.

	ΔT2 (°C)	ΔWS10 (m s^{-1})	ΔRH2 (%)	ΔPBL height (m)	Δ$PM_{2.5}$ (μg m^{-3})	ΔK_z (m^2 s^{-1})
			Study period (17 February to 12 March)			
All day	-1.4 (-69.4%)	-0.038 (-3.1%)	+8.7 (+14.9%)	-160.0 (-18.6%)	+20.0 (+28.6%)	-3.3 (-27.0%)
Daytime	-1.8 (-42.1%)	+0.028 (+1.9%)	+9.0 (+16.9%)	-267.1 (-22.4%)	+21.1 (+35.6%)	-6.7 (-27.6%)
			First haze episode (20–26 February)			
All day	-1.8 (-59.7%)	-0.52 (-19.5%)	+9.8 (+12.4%)	-183.6 (-31.0%)	+45.1 (+38.7%)	-3.9 (-48.8%)
Daytime	-2.5 (-46.6%)	-0.59 (-19.8%)	+10.4 (+13.8%)	-307.3 (-37.6%)	+49.3 (+48.5%)	-8.3 (-51.9%)

Table 6. Same as Table 5 but for Beijing.

	ΔT2 (°C)	ΔWS10 (m s^{-1})	ΔRH2 (%)	ΔPBLH (m)	Δ$PM_{2.5}$ (μg m^{-3})	ΔK_z (m^2 s^{-1})
			Study period (17 February to 12 March)			
All day	-1.6 (-39.1%)	-0.48 (-13.9%)	+11.8 (+23.3%)	-154.0 (-18.3%)	+30.1 (+29.8%)	-4.5 (-37.5%)
Daytime	-2.3 (-33.1%)	-0.52 (-13.9%)	+12.5 (+28.1%)	-282.7 (-22.5%)	+34.0 (+43.9%)	-9.6 (-38.8%)
			First haze episode (20–26 February)			
All day	-2.1 (-46.1%)	-0.58 (-20.4%)	+17.0 (+24.5%)	-195.6 (-35.9%)	+68.0 (+39.1%)	-5.0 (-59.5%)
Daytime	-3.4 (-44.6%)	-0.78 (-23.9%)	+17.9 (+27.2%)	-358.3 (-45.5%)	+83.2 (+59.6%)	-11.0 (-63.2%)

Table 7. The model simulated feedback-induced changes (FULL minus NoAFB) in BC, sulfate (SO_4^{2-}) and nitrate (NO_3^-) averaged over the BTH region and Beijing during the entire period and the first haze episode. Inside the parentheses are percentage changes relative to the NoAFB case.

	Beijing-Tianjin-Hebei region (BTH)			Beijing		
	ΔBC (μg m^{-3})	ΔSO_4^{2-} (μg m^{-3})	ΔNO_3^- (μg m^{-3})	ΔBC (μg m^{-3})	ΔSO_4^{2-} (μg m^{-3})	ΔNO_3^- (μg m^{-3})
			Study period (17 February to 12 March)			
All day	+0.9 (+25.1%)	+5.0 (+46.4%)	+6.8 (+37.3%)	+1.6 (+27.5%)	+8.4 (+58.5%)	+8.4 (+36.9%)
Daytime	+1.0 (+39.5%)	+5.4 (+60.2%)	+7.2 (+43.2%)	+1.9 (+51.5%)	+9.5 (+86.5%)	+9.5 (+48.8%)
			First haze episode (20–26 February)			
All day	+1.9 (+32.9%)	+12.6 (+66.9%)	+14.6 (+40.9%)	+3.1 (+33.6%)	+22.3 (+81.8%)	+16.7 (+34.7%)
Daytime	+2.2 (+50.1%)	+13.8 (+81.4%)	+15.8 (+48.3%)	+4.1 (+62.3%)	+26.0 (+112.4%)	+20.9 (+51.5%)